PROTON RADIATIVE CAPTURE BY TRITIUM BELOW 30 MeV

By

ROBERT CHISM McBROOM

A DISSERTATION PRESENTED TO THE GRADUATE COUNCIL OF
UNIVERSITY OF FLORIDA
IN PARTIAL FULFILLMENT OF THE REQUIREMENTS FOR THE
DEGREE OF DOCTOR OF PHILOSOPHY

UNIVERSITY OF FLORIDA

1977

ACKNOWLEDGEMENT

This project was conducted under the guidance of Dr. H. R. Weller. His patience and direction are deeply appreciated. A special thanks to Dr. N. R. Roberson and the members of the Duke Capture Gamma Group for the privilege of working with them. The author is especially grateful for the Group's assistance with the acquisition of the experimental data. Thanks to Dr. C. P. Cameron for the use of some of his computer programs. Also, thanks to Mrs. M. Bailey for her care in drafting the figures, Mr. D. Turner for the photography, and Mrs. J. Ogden for the typing. The author is thankful to Mr. D. C. Pound and The General Atomic Company for their support during the final stages of the dissertation.

Financial support for this study was provided by the University of Florida.

Final and most heartfelt thanks to the author's wife, Mrs. Karen McBroom, for her love throughout all the trials.

TABLE OF CONTENTS

LIST OF TABLES

LIST OF FIGURES

Abstract of Dissertation Presented to the Graduate Council of the University of Florida in Partial Fulfillment of the Requirements for the Degree of Doctor of Philosophy

PROTON RADIATIVE CAPTURE BY TRITIUM BELOW 30 MeV

By

Robert Chism McBroom

June 1977

Chairman: Henry R. Weller
Major Department: Physics

The $^{3}H(p,\gamma)^{4}He$ reaction is studied for incident proton energies from 8-30 MeV. The experimental data is composed of excitation functions measured at the angles of 55^{o}, 90^{o} and 125^{o} in the center of mass system in 1 MeV steps from 8-15 MeV proton energy and in 0.5 MeV steps from 17-30 MeV proton energy. These data measured the energy dependence of the cross section and its deviation from the sin θ angular dependence of the electric dipole (E1) radiation.

Additional angular distributions were taken at selected energies in the range from 13-30 MeV with up to nine angles measured between 20^{o} and 142^{o} in the laboratory.

This number of angles was taken to insure statistical significance for determining the coefficients of the Legendre expansion of the differential cross section through a_4. The experimental data is shown to be consistent with the assumption that the observed radiation is primarily E1 with an additional electric quadrupole (E2) component and negligible contributions from higher order multipoles. The E2 radiation is shown to be consistent with a model of the E2 cross section composed of the sum of a direct interaction component, and two Breit-Wigner resonances. A resonance of width 12 MeV at a ^{4}He energy of 35 MeV is observed in agreement with previous experimenters and a second previously unobserved resonance is observed with a width of 3.8 MeV at a ^{4}He energy of 39.5 MeV.

INTRODUCTION

Investigations of the properties of the ^{4}He nucleus are an important method of improving the understanding of the nuclear force. Consisting of four nucleons, ^{4}He falls in a transition region between describing the nuclear interaction in terms of nucleon-nucleon interactions and statistical descriptions of many nucleon interactions. The properties of the ^{4}He nucleus show a number of differences from predictions based on the two-nucleon interaction and the assumption that the two-nucleon forces are additive. Similar difficulties are observed with models that are based on systems with a large number of nucleons.

The application of models of the nuclear interaction to ^{4}He seeks to predict the observed properties of this nucleus. One of these properties is the fact that ^{4}He is the most tightly bound of all the nuclei.[1] Another property to be considered is the root-mean-square (rms) charge radius measured using the elastic scattering of electrons.[2-4] Indications of the presence of many body forces are obtained in measurements of the charge distribution of the nucleus by electron scattering. The charge distribution deviates significantly from a Gaussian shape.[4]

Also to be considered in a description of ^{4}He is evidence that the ground state is not a pure spin zero (S=0) shell model state.[5]

Many models have been presented to describe the observed properties of ^{4}He. Their success has been varied. In general the models proceed by incorporating short range correlations and non-central forces into the interaction.[6-7] Further information on the importance of ground state correlations is sought from the angular distributions of ^{4}He photonuclear reactions.[9]

Several measurements of the ^{4}He photonuclear reactions have been made. A number of inconsistencies were observed in the early works, some of which have been resolved by more recent measurements. The behavior of the angular distributions has been interpreted to give supporting evidence for the presence of ground state correlations.[10-12] In addition, evidence exists for the presence of resonant excited states in ^{4}He whose influence should be considered in a complete description of the angular distributions.[13,14]

Evidence for excited states in ^{4}He is presented in the analysis of many experiments. This evidence is derived primarily from reactions in which ^{4}He is formed as the compound nucleus.[15] Evidence for several states has been obtained from phase shift analyses of nucleon scattering data. Other states are seen in inelastic electron scattering.[16,17] All of these states have positive energy.

There exists no evidence for bound states of ^{4}He. Isospin selection rules indicate that the photodisintegration of ^{4}He can be useful in the investigation of negative parity, $J^\pi = 1^-$, isospin T = 1 states and positive parity $J^\pi = 2^+$, T = 0, 1 states. Some studies of the ^{4}He $(\gamma,p)^3$H reaction have exhibited resonance-like structures, but ^{3}H $(p,\gamma)^4$He measurements have failed to confirm the existence of the proposed levels.[18-21] Measurements of the ^{4}He $(\gamma,n)^3$He reaction present evidence for a $J^\pi = 2^+$, T = 0 resonance at a gamma energy of $E_\gamma \sim$ 35 MeV.[22] It will be shown that the present work provides additional evidence for the existence of this level at 35 MeV in ^{4}He.

Most of the ^{4}He photodisintegration experimental efforts for excitation energy in the range from 20-40 MeV have been devoted to the ^{4}He $(\gamma,n)^3$He reaction. The early studies of the ^{4}He $(\gamma,p)^3$H reaction suffered from difficulties due to poor statistics. For energies below 35 MeV where the triton tract becomes too short to measure, the diffusion chamber and cloud chamber measurements have difficulty distinguishing protons which arise from multiparticle final states.[11,12] Studies of the inverse reaction ^{3}H $(p,\gamma)^4$He have been conducted for limited excitation energy ranges from 20 MeV to 34 MeV. In the present experiment measurements of the energy and angular dependence of the ^{3}H $(p,\gamma)^4$He reaction were taken for excitation energies from 26 to 42 MeV.

The proton beam from the Triangle Universities Nuclear Laboratory Cyclo-Graaff was used to provide incident protons in the energy range from 8 to 30.5 MeV. The beam was incident on a 5μ self-supporting tritiated titanium foil target containing about 0.14 mg/cm^2 of tritium. The emitted photons were detected with a thallium doped sodium iodide NaI(TI) detector for up to nine laboratory angles between 20^o and 142^o. It will be shown that these measurements indicate the existence of a previously unobserved level in ^{4}He at about 40 MeV excitation having a J^π of 2^+ and a width of about 3 MeV in the center of mass.

An appendix is included which describes a peak fitting program. This program was designed to extract the low energy tail of the NaI detector response curve from beneath the peaks due to gamma rays from transitions to states other than the ground state. The shape of the NaI response curve was based on the measured response to the ^{3}H (p,γ)^{4}He reaction.

CHAPTER I
SUMMARY OF LITERATURE

The ^{4}He nucleus has been the subject of intense interest. The resulting body of literature is extensive in both experimental and theoretical studies. This body of literature is reviewed in a number of recent works, particularly the survey by Fiarman and Meyerhof (1973).[15] Many different theoretical models have met with qualitative success in describing the observed ground state properties of ^{4}He, but have been unable to satisfactorily describe all the observed properties. Further input for model determination is provided by experimental studies of the excited states of ^{4}He. While there are no bound states of ^{4}He, experimental evidence exists for virtual states as shown in Figure 1.1. Particular consideration is given here to the photon excitation states having spin and parity (J^π) and isopin (T) quantum numbers as follows:

$J^\pi = 1^-$, $T = 1$ and

$J^\pi = 2^+$, $T = 0,1$

These states have been studied by photodisintegration and the inverse photonuclear reaction. The experimental results to date have not definitively established the

Figure 1.1 Excited States of ^{4}He. The energy levels of ^{4}He and the general form of the cross sections for the four reactions, which form ^{4}He as the compound nucleus, are shown (Fiarman and Meyerhof[15]).

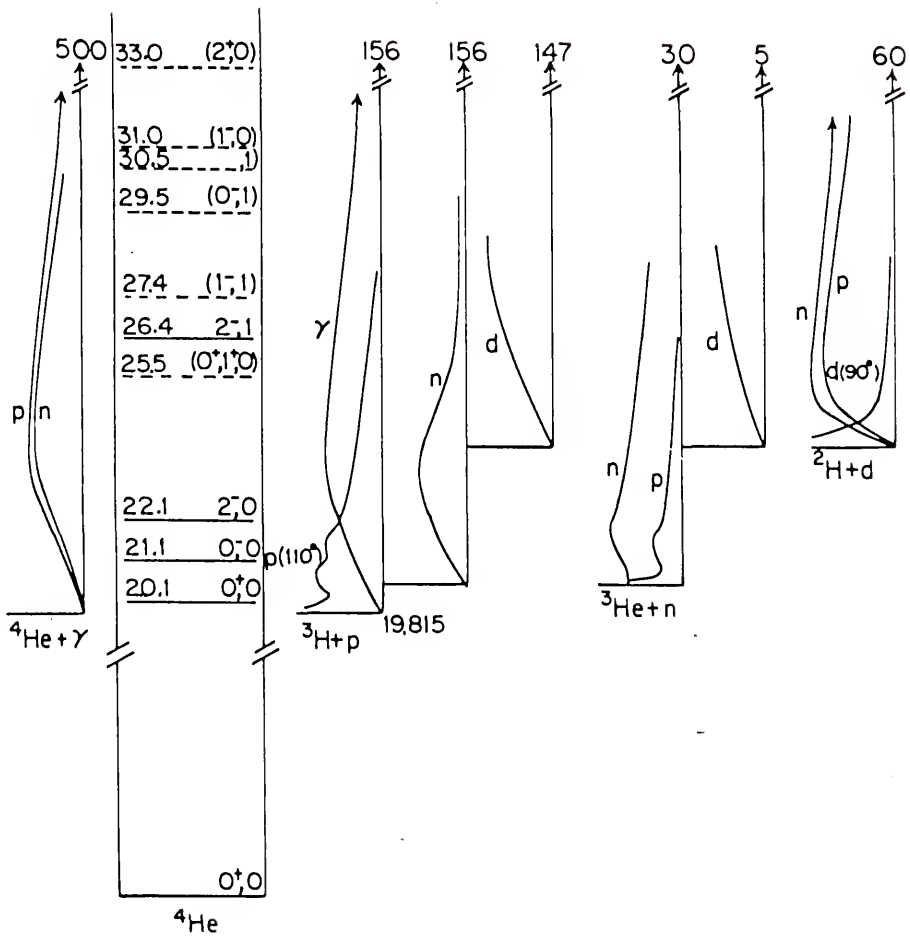
500
33.0 (2+,0)
31.0 (1-,0)
30.5 (1-,1)
29.5 (0-,1)
27.4 (1-,1)
26.4 2-,1
25.5 (0+,1+,0)
22.1 2-,0
21.1 0-,0
20.1 0+,0
0+,0
4He
p
n
4He + γ
156
γ
p(110°)
3H + p
19.815
156
n
147
d
30
n
p
3He + n
5
d
60
n
p
d(90°)
2H + d

existence of any of these states; although studies of the $^{4}He(\gamma,n)^{3}He$ reaction indicate the existence of a $J^{\pi} = 2^{+}$, $T = 0$ state for an excitation energy of 35 MeV.[22] In addition to the question of the existence of excited states, there are fundamental questions regarding the observed shapes of the photoproton and photoneutron angular distribution as a function of the gamma ray energy. The (γ,n) distribution is predicted to be backward peaked while experimentally it is observed to be forward peaked for excitations less than 27 MeV and then to become backward peaked between 27 and 35 MeV excitation.[22] For energies greater than 35 MeV excitation the angular distribution of the (γ,n) reaction is forward peaked and the asymmetry approaches the asymmetry of the (γ,p) reaction channel.[10-12] The (γ,n) forward peaking may be interpreted to be due to correlations in the ground state wave functions.[23]

The experimental observations of the photodisintegration reaction have limited resolution. These measurements are averaged quantities in a given energy interval. One method of relating these averaged quantities to the properties of the Hamiltonian and the ground state wave function is the sum rule approach.[24] The theory of sum rules has undergone extensive development starting from the study of atomic photoabsorption processes. For the electric dipole (E1) radiation in the long wave length

approximation the integrated cross section is given by the sum rule

$$\begin{aligned} \sigma_{\text{int}}^{\text{El}} &= \int_0^\infty \sigma^{\text{El}}(\varepsilon)\, d\varepsilon \\ &= \sum_k e_k^2 \, \langle 0 | \, [Z_k, [H, Z_k]] \, | 0 \rangle \\ &\geq 60 \, \frac{NZ}{A} \quad (= 60 \text{ MeV - mb for } {}^4\text{He}).^{24} \end{aligned} \tag{1.1}$$

The wave vector $|0\rangle$ is the ground state wave function, H is the nuclear Hamiltonian, Z_k the position operator, and e_k is the effective charge for the kth nucleon. The equality in the last term is satisfied if the position operator commutes with the potential energy operator. This condition is violated by Majorana or Heisenberg exchange forces or velocity dependent forces. Each of these three interactions would tend to increase $\sigma_{\text{int}}^{\text{El}}$. Electron scattering experiments indicate that the contribution due to exchange currents may be included as follows:

$$\sigma_{\text{int.}}^{\text{El}} = 60 \, \frac{NZ}{A}(1 + a), \; a = 0.40.^{25\text{-}27} \tag{1.2}$$

$$(= 84 \text{ MeV-mb for } {}^4\text{He})$$

Under the assumption that the ground state is spatially symmetric and including the charge radius of the proton, the Levinger, Bethe (28) bremsstrahlung-weighted cross section is related to the nuclear radius by the following dipole sum rule:

$$\sigma_b^{El} = \int_0^\infty \frac{1}{E} \sigma^{El}(E)\,dE$$

$$= 0.096 \frac{NZ}{A-1} (R_z^2 - R_p^2)$$

(= 2.48 mb for ^{4}He)

where R_z and R_p are the nuclear and proton rms radii respectively.[29-41]

The quantity $\sigma^{El}(E)$ referred to in the sum rules is the total cross section for all electric dipole photodisintegrations. For the ^{4}He reactions there are five competing reactions. The yields for these five reactions were measured by Gorbunov and co-workers.[10,11] A 170 MeV Bremsstrahlung beam incident on a cloud chamber was used in the study. Their results for the relative yield of the various reactions are shown in Table 1.1.

The measured angular distributions indicated that the El interaction comprises ∿94% of the total integrated cross section up to 170 MeV. Approximating σ^{El} by the total cross section, integration of Gorbunov's data for the reactions of Table 1.1 gives:

$$\sigma_{int.}^{El} = 95 \pm 7 \text{ MeV mb and } \sigma^{El} = 2.4 \pm .15 \text{ mb}$$

This value is larger than that predicted by the simple sum rules (Eq. 1.1-1.3) indicating contributions due to exchange and velocity dependent forces. When these forces are considered as in the sum rule analysis of Quarati[34]

Table 1.1

^{4}He Photodisintegration Reactions

Reaction	Threshold Energy (MeV)	Relative Yield	Quatri Sum Rule	Sum of Shell Model Level Strength 0-50M
^{4}He(γ,p)^{3}H	19.8	1.0[a]		
^{4}He(γ,n)^{3}He	20.6	1.0[b]		
^{4}He(γ,pn)^{2}H	25.9	.26[c]		
^{4}He(γ,2p2n)	28.2	.07[c]		
^{4}He(γ,d)^{2}H	23.7	.002[d]		
^{4}He +		95mb-MeV[g]	100mb-MeV[e]	108mb-MeV[f]

a. Arkatov, et al.[32] E_γ (Max) = 120 MeV

b. Gorbunov[10] and Gorbunov and Spiridonov.[11] E_γ (Max) = 170 MeV

c. Arkatov, et al.[33]

d. Meyerhof, et al.[34]

e. Quarati.[35]

f. Szydlik, et al.[36]

g. Malcom.[41]

for the shell model (Table 1.1), the experimental cross section up to 170 MeV excitation exhausts 95% of the sum rule.

These results indicate the usefulness of sum rules. This usefulness may be increased by the removal of the approximation that the total cross reaction is due to the E1 interaction. In Table 1.2 are listed the sum rules commonly appearing in the literature along with their representations in the shell model formulism. The results of these equations for the shell model parameters are $\beta = 1.75$ fm^2, $k_{E1} = \frac{1}{5.4}\text{fm}^{-1} = 36$ MeV and $k_{E2} = \frac{1}{2.5}\text{fm}^{-1}$ These values give the rms charge radius of ^{4}He to be $\langle r_{^4He}\rangle^{\frac{1}{2}} = 1.62$ fm. It has been suggested by Leonardi and Lipparini[38] that the final entry in Table 1.2, σ_{-3}, be measured, as the σ^{E2}_{-3} sum rule for the electric quadrupole strength is dependent only on the ground state wave function.

These features of the four nucleon system have received extensive theoretical treatment. Many different models have been successful to varying degrees in describing these features. The common factor in most of these analyses is an attempt to develop a method to properly account for the contributions of many body and velocity dependent forces in an orderly way. Many of the models are based on "realistic" potentials that are derived from

Table 1.2

Sum Rules for ^{4}He and Their Shell Model Representation.[35]

Sum Rule	Shell Model Representations	Experimental* Values
$\sigma_{int} = \int\sigma(\omega)d\omega$	$=\pi^2e^2(2\beta^{-1}k_{E1} + \frac{1}{4}\beta^{-2}\ k_{E2}^3)$	$= 19.5 \pm .07 fm^2 MeV$
$\sigma_b = \frac{\int\sigma(\omega)d\omega}{\omega}$	$= \frac{\pi^2e^2}{197.26}\ (2\beta^{-1} + \frac{1}{4}\beta^{-1}\ k_{E2}^2)$	$= 0.024 \pm .015 fm^2$
$\sigma_\alpha = \int\sigma(\omega)\omega d\omega$	$= 197.26\ \pi^2e^2\ (2\beta^{-1}\ k_{E1}^2 + \frac{1}{4}\beta^{-2}\ k_{E2}^4)$	$= 492 \pm 4.8 fm^2 MeV^2$
$\sigma_{-2} = \frac{\int\sigma(\omega)d\omega}{\omega^2}$	$= \frac{\pi^2e^2}{(197.26)^2}(2\beta^{-1}\ k_{E1}^{-1} + \frac{1}{4}\beta^{-2}\ k_{E2})$	$= 0.0073 \pm .00004 fm^2/MeV$
$\sigma_{-3} = \frac{\int\sigma(\omega)d\omega}{\omega^3}$		

$\sigma(\omega) = \sigma_{E1}(\omega) + \sigma_{E2}(\omega)$ - experimental cross section

Table 1.2 (continued)

Sum Rule	Shell Model Representations	Experimental* Values

$\omega = E_\gamma / k$

k_{EL} - average energy of all the transitions from the gound state to states of the discrete or continuous spectrum allowed by the electric multipole operator of order L.

β - Harmonic oscillator parameter $M\omega(fm^{-2}) = \left(\frac{2}{3}\int R_{oo} r^2 R_{oo} r^2 dr\right)^{-1}$

$R_{oo} = \left(\frac{2}{\Gamma(\frac{1}{2})^3}\right)^{\frac{1}{2}} \beta^{3/4} \exp(-\frac{1}{2}\beta r^2) L_{\frac{1}{2}}^{\frac{1}{2}}(\beta r^2)$

$L_{\frac{1}{2}}^{\frac{1}{2}}(\beta r^2)$ - Laguerre polynomial

* Numerical Values from Experimental Work by Gorbunov.[10,11]

the nucleon-nucleon scattering phase shifts.[7,8,39,40] These potentials fit the on-shell matrix elements equally well. Their differences are embodied in their treatment of off-shell matrix elements. One such potential is the Sussex potential which was used by Szydlik, et al.[36] to calculate the spectrum of ^{4}He.

Photodisintegration studies of the ^{4}He nucleus span the excitation energy range from threshold to 500 MeV. The reaction is characterized by the asymmetries in the proton and neutron angular distributions. At low excitation energies the asymmetries exhibit structure which has been interpreted as being due to interference between the electric dipole (El) and electric quadrupole (E2) absorption amplitudes.[22,41] For excitations above 100 MeV the (γ,n) and (γ,p) asymmetries approach one another.[42] The absorption of photons of energies of 100 MeV or higher is expected to occur predominantly by the quasideuteron mechanism discussed by Levinger.[9] Recent calculations by Gari and Hebach account well for the total cross section and asymmetry in the range $50 \leq E \leq 140$ MeV.[23]

Many measurements have been made of the various ^{4}He photodisintegration processes. An overview of these experiments is shown in Table 1.3. The history of the experimental measurements is one of controversy.[41-44] The early measurements gave the general character of the energy and

Table 1.3

^{4}He Experimental Studies

	Experimental Group (First Author)	Detection Method	Excitation Energy MeV	Ang. Dist.	σMax. mb	Reported Structure E_{res} MeV
(γ,n)	Ferguson ('54)[43]	thermal n to BF_3	21-26	90°	1.3	
	de Saussure ('55)[44]	emulsions	40-120	yes		
	Livesey ('58)[45]	emulsions	40-60	yes		
	Ferrero ('66)[46]	thermal n to BF_3	21-80	4π	1.3	24, 28
	Arkatov ('69)[47]	diff. chamber 8 atm	34-120	yes		
	Busso ('70)[48] Busso ('70)[49]	diff. chamber 5 atm	25-60	yes	1.1	28
	Berman ('70)[50]	thermal n to BF_3	21-32	Fore-Aft	1.0	26, 28

Table 1.3 (continued)

	Experimental Group (First Author)	Detection Method	Excitation Energy MeV	Ang. Dist.	σMax. mb	Reported Structure E_{res} MeV
	Berman ('71)[51]	time of flight	21-32		1.0	26,28
	Berman ('70)[52]	time of flight	21-32	90^{o}	.9	
	Malcom ('72)[22]	time of flight	24-72	yes		35
	Irish ('73)[53]	time of flight	21-40	90^{o}		
	Irish ('75)[54]	time of flight	20-34	yes		
	Arkatov ('75)[55]	diff. chamber 1.5 atm.	27-30	yes		
(p,γ)	Perry ('53)[56]	NaI scint.	19.8-23	$0^{o}.90^{o}$		
	Shrack('65)[57]	NaI scint.	20.5-22.6	yes		26
	Perry ('55)[20]	NaI scint.	21-25	yes	1.8	
	Gardner ('62)[21]	NaI scint.	24-27	yes	1.7	

Table 1.3 (continued)

	Experimental Group (First Author)	Detection Method	Excitation Energy MeV	Ang. Dist.	σMax. mb	Reported Structure E_{res} MeV
	Gemmel ('62)[58]	NaI scint.	23-28	yes	1.8	
	Didilez ('68)[59]	NaI scint.	135	yes		
	Meyerhof ('70)[13]	NaI scint.	22-34	yes	1.8	
	Glavish ('72)[60]	NaI scint.	24-30	yes	1.8	
(γ,n) & (γ,p)	Gorbunov ('58)[10] ('68)[11]	cloud chamber	22-260	yes	p 1.8 n 1.8	
	Busso ('71)[61]	diff. chamber 5 atm.	22-80	yes	p 1.7 n 1.1	25, 28 25, 28
	Argan ('75)[62]	telescope spectrometer	150-450	60^{o},90^{o}		
(e,e' ^{3}H) & (e,e' ^{3}He)	Wait ('70)[12]	spectrometer	30-85	yes		
	Dodge ('72)[63]	spectrometer	30-52	yes		

Table 1.3 (continued)

	Experimental Group (First Author)	Detection Method	Excitation Energy MeV	Ang. Dist.	σMax. mb	Reported Structure E_{res} MeV
(γ,p)	Fuller ('54)[64]	emulsions	21-40	yes	1.8	
	Milone ('60)[18]	emulsions	21-32	90	1.8 24.7	26,27,28
	Main ('62)[65]	emulsions	23-32	yes		
	Clerc ('65)[66]	spectrometer	24-56	90	1.7	
	Mundhenke ('68)[67]	spectrometer	21-33	90	1.4	26, 28
	Denisov ('68)[68]	counter telescopes	21-52	90	1.5	26
	Arkatov ('71)[33]	diff. chamber 10 atm.	20-120	yes	1.8	26.5,28.7, 31
$^4He(e,d)e^+ \ ^2H$	Skopik ('72)[69]	spectrometer	36-50	yes	3.2×10^{-3}	
$^4He(\gamma,d)^2H$	Asbury ('65)[70]	counter telescope	220-265	52		

Table 1.3 (continued)

	Experimental Group (First Author)	Detection Method	Excitation Energy MeV	Ang. Dist.	σMax. mb	Reported Structure E_{res} MeV
	Arkatov ('73)[71]	diff. chamber	44-65	yes		
$^{2}H(d,\gamma)^{4}He$	Akimov ('62)[72]	counter telescope	220			
	Poirer ('63)[73]	counter telescope	247	135		
	Zurmuhle ('63)[74]	NaI scint.	20.5-25	45		
	Meyerhof ('69)[34]	NaI scint.	27-33	yes	3.3×10^{-3}	
	Degre ('71)[75]	NaI scint.	24-26	yes		
	Poutisson ('73)[76]	NaI scint.	29-35	Yes		

angular dependence of the excitation. For the cloud chamber and diffusion chamber results there are difficulties relating to small numbers of events in a given excitation range and in analyzing the tracks of the product particles for excitations below 30 MeV. Particular difficulty is associated with the measurement of the ^{3}He recoil for the (γ,n) measurement. All the photodisintegration experiments suffer from difficulties associated with the spectral distribution of the photon beam. These early measurements indicated the existence of a number of structures in the cross sections, but could give little definitive information concerning the (γ,n) assymmetry.

The measurements by the different experimenters are in general agreement concerning the magnitude of the (γ,p) cross section. However, the (γ,n) cross section is quite variable. Charge independence considerations support the results obtained by Gorbunov that the (γ,n), (γ,p) cross sections are the same.[11,77-80] The measurements are in agreement for an excitation energy greater than 35 MeV. The results reported by Berman, et al.[50-52] and Busso, et al.[48,49], give a lower (γ,n) cross section for energies between 23 and 35 MeV. In the case of Berman's results, the cross section would agree with the measurements of Gorbunov[10] if multiplied by a factor of 1.8.[41] This disagreement has been clarified by a series of experiments by Irish, et al.[53,54] which show that the variation was

due to a reduced target thickness from bubble formation in liquid ^{4}He.[80] Measurements with liquid targets by Malcom, et al.[22] give the (γ,n) cross section in agreement with Gorbunov. The 5 atm diffusion chamber measurements by Busso agree with other experimenters for excitations above 30 MeV but fall below the (γ,p) cross section at lower excitation. Recent 1.5 atm diffusion chamber measurements by Arkatov, et al.[55] with improved accuracy in the low energy ^{3}He recoil measurement give the (γ,n) cross section in agreement with the (γ,p) cross section. These results for the ^{4}He (γ,p) and (γ,n) cross sections give experimental evidence for the charge independence of the nuclear force.[79]

The existence of evidence for excited states of ^{4}He has been reported by many experimenters as seen in Table 1.3. There is little agreement in the structure seen by various early experimenters. The recent experiments with better statistics exhibit much less structure than seen previously. The experimental cross sections are shown in Figure 1.2. The significant features are the peak of the cross section for an excitation energy of 26 MeV and a broad peak for 28 MeV excitation. Peaks in this region are consistent with the existence of two states with angular momentum, parity $J\pi = 1^-$ and isospin T = 1. These states correspond to a mixture of the spectroscopic states singlet $^1P_1$ and triplet $^3P_1$.[13]

Figure 1.2 ^{4}He Photodisintegration Cross Sections. This figure is a compilation of the results reported by the indicated authors.

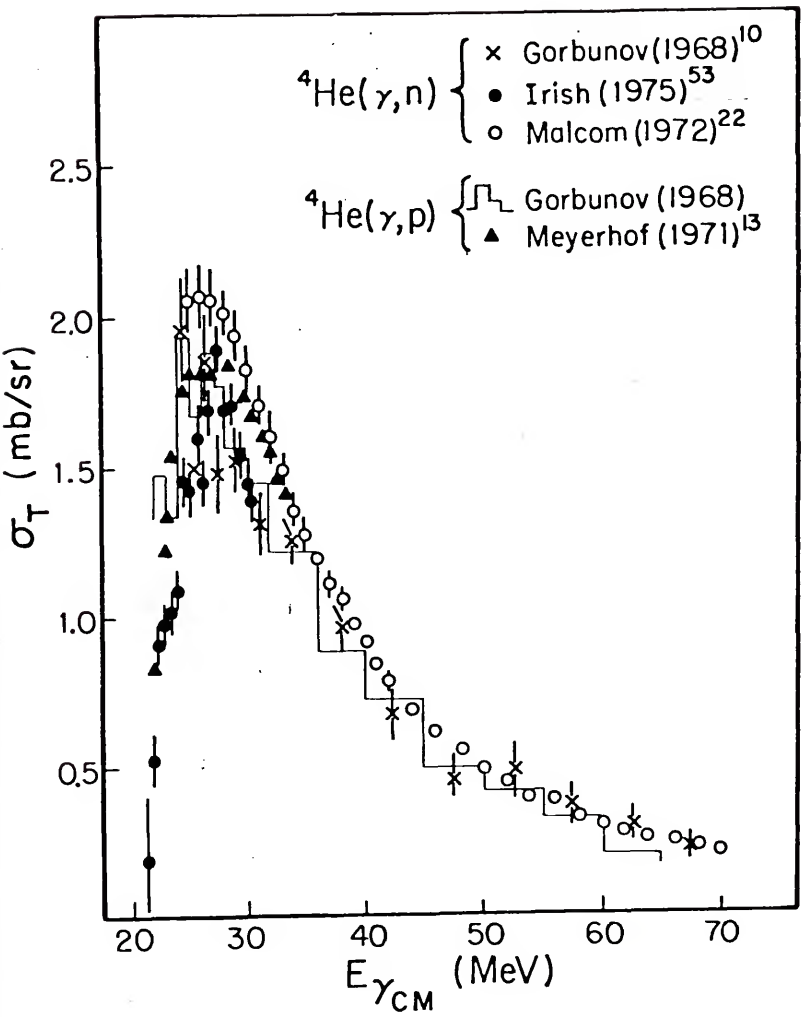
$^4He(\gamma,n)$
× Gorbunov(1968)[10]
• Irish (1975)[53]
o Malcom (1972)[22]
$^4He(\gamma,p)$
Gorbunov (1968)
▲ Meyerhof (1971)[13]
σ_T (mb/sr)
2.5
2.0
1.5
1.0
0.5
20
30
40
50
60
70
$E_{\gamma_{CM}}$ (MeV)

Evidence for a third excited state at 35 MeV excitation with angular momentum, parity $J^{\pi} = 2^{+}$ and isospin T = 0 is obtained from (γ,n) asymmetry measurements.[22]

The (γ,n) and (γ,p) angular distributions are given in terms of the Legendre polynomial expansion as

$$\frac{d\sigma}{d\Omega} = A_o \left(1 + \sum_k a_k P_k (\cos \theta)\right).[81] \qquad (1.4)$$

The coefficients contain contributions from photons of multipolarity L for $k \leq 2L$, k even and $k \leq L + L^1$, k odd where L^1 is the multipolarity of an interfering photon. The equivalent expansion in terms of sin θ and cos θ prevalent in the literature is

$$\frac{d\sigma}{d\Omega} = B(\alpha + \sin^2 \theta + \beta \sin^2 \theta \cos \theta + \delta \sin^2 \theta \cos^2 \theta + \varepsilon \cos \theta + \ldots) \qquad (1.5)$$

The coefficients $B\alpha$, B, $B\beta$, $B\delta$ and $B\varepsilon$ correspond to amplitudes and cross terms for multipolarities of 0, 1, and 2. The respective relations between the coefficients of the two expansions are shown in Table 1.4. Electric operators involve only space coordinates and magnetic operators only spin coordinates in the central force approximation. For a pure ^1S_o ground state the allowed final states of the outgoing particles are $^3S_1$, $^1P_1$, and $^1D_2$ for angular momentum changes less than two. The admixture of D states in the ground state indicated by variational calculations and

Table 1.4

Relations Between the Legendre Polynomial and sin θ, cos θ Angular Distribution Expansions

$$B = A_o \left(\frac{-3}{2} a_2 - \frac{5}{8} a_4 + \ldots\right)$$

$$\alpha = \frac{1 + a_2 + a_4 + \ldots}{\frac{3}{2} a_2 - \frac{5}{8} a_4 + \ldots}$$

$$\beta = \frac{\frac{-5}{2} a_3 - 7a_5 + \ldots}{\frac{-3}{2} a_2 - \frac{5}{8} a_4 + \ldots}$$

$$\delta = \frac{-\frac{35}{8} a_4 + \ldots}{\frac{-3}{2} a_2 - \frac{5}{8} a_4 + \ldots}$$

$$\varepsilon = \frac{a_1 + a_3 + a_5 + \ldots}{\frac{-3}{2} a_2 - \frac{5}{8} a_4 + \ldots}$$

^{4}He (p,p) ^{4}He measurements complicates the interpretation of the coefficients of the angular distribution. Possible additional contributions may be observed as an increase in the isotropic component from E1 transitions from the D state to P and F states and a contribution from the cos θ term which arises from interference between E1 and non-spin-flip M1 transitions.[41] The angular distribution measurements by Wait[12], Gorbunov[10] and Meyerhof[13] yield negligible values for the coefficients α and ε. Their results are dominated by the E1 term B.

The asymmetry (a_s) of the angular distributions about $\theta = 90^o$ can be defined in terms of the difference between the cross section at 55^o and 125^o. This quantity, as will be shown in Chapter II, can be written as

$$a_s = a_1 + \frac{P_3 (\cos 55^o)}{P_1 (\cos 55^o)} a_3 = a_1 - .68\ a_3$$

for the Legendre polynomial expansion (or equivalently the term β for the sin θ, cos θ expansion) where $P_2(\cos 55^o) = 0$ eliminating a_2. These terms arise from interference between the electric dipole and quadrupole interactions. At low energy the observed angular distributions are very close to a pure sin θ distribution.[56] This distribution indicates a predominately dipole interaction. The isotropic terms were observed by Gorbunov to be small for photon energies up to 170 MeV providing a basis for the assumption that only E1, E2

radiation contribute significantly to the yield. The interference terms producing the asymmetry are more sensitive to smaller amounts of E2 interaction than the E2 amplitude itself under these conditions. This result is due to the fact that the coefficients a_1 and a_3 are proportional to the product of the dipole and quadrupole amplitudes.

CHAPTER II
EXPERIMENTAL METHODS AND MEASUREMENTS

This study consists of a series of experimental measurements designed to obtain the electric quadrupole E2 strength as a function of the excitation of the compound nucleus for the reaction $^{3}H(p,\gamma)^{4}He$. The methods used to determine the E2 strength consisted of measuring the asymmetry of the angular distribution about 90^{o} and the measurement of the detailed angular distributions of the outgoing γ-rays. Shell model calculations predict a number of states of angular momentum and parity $J^{\pi} = 2^{+}$ with isospin T = 0,1 in the energy range from 30-50 MeV excitation. The proton energies available from the Triangle Universities Nuclear Laboratory (TUNL) Cyclo-Graaff allow study of the energy range from 22 to 42 MeV excitation of the compound nucleus.

Experimental Details

Using a 15 MeV isochronous Cyclotron as a source, the TUNL FN Tandem provides a pulsed 25 MHz proton beam. The beam energy is continuously variable from 17-31 MeV. The beam pulse width is 2 ns and the energy spread is 30 KeV. The root-mean-square beam current delivered to the target was kept in the range of 20 to 100 nanoamperes depending on

the total count rate in the sodium iodide detector. The count rate in the detector was kept below 350k counts per second because pile-up problems and a deterioration of the resolution occurred for higher count rates.

Two separate detector assemblies were used in the experiment. The first detector assembly was a high resolution system and was used for the yield curve measurements and the angles of the angular distributions between 42^{o} and 142^{o}. The second detector assembly allowed measurements to be obtained for angles between 10^{o} and 90^{o} although with reduced resolution. The experimental arrangement was designed in both cases to minimize the background events that were not associated with the target.

The detector assembly is based on a cylindrical 25.4 x 25.4 cm thallium doped sodium iodide crystal. This crystal is surrounded by a well type Ne 110 plastic scintillator. The center crystal is viewed by six RCA-8575 photomultiplier tubes and the plastic scintillator by eight XP1031 photomultiplier tubes.[82] A schematic of the detector arrangement is shown in Figure 2.1. Active shielding is provided by detecting coincidences between the plastic detector and the center-crystal detector which were processed by the electronics to reject cosmic ray events. Passive shielding for the detector is provided by four inches of lead and eight inches of paraffin loaded with lithium carbonate (∿50% by weight). The detector is mounted on a carriage that allows

Figure 2.1 Detector Assembly for 25.4 x 25.4 cm Cylindrical NaI(Tl) High Resolution Detector. This illustration shows the arrangement of the active and passive shielding from the cosmic rays and beam associated background. The collimator arrangement that was used to restrict the cone of gamma rays to that just illuminating the back face of the detector crystal is shown (Weller, et al.[82]).

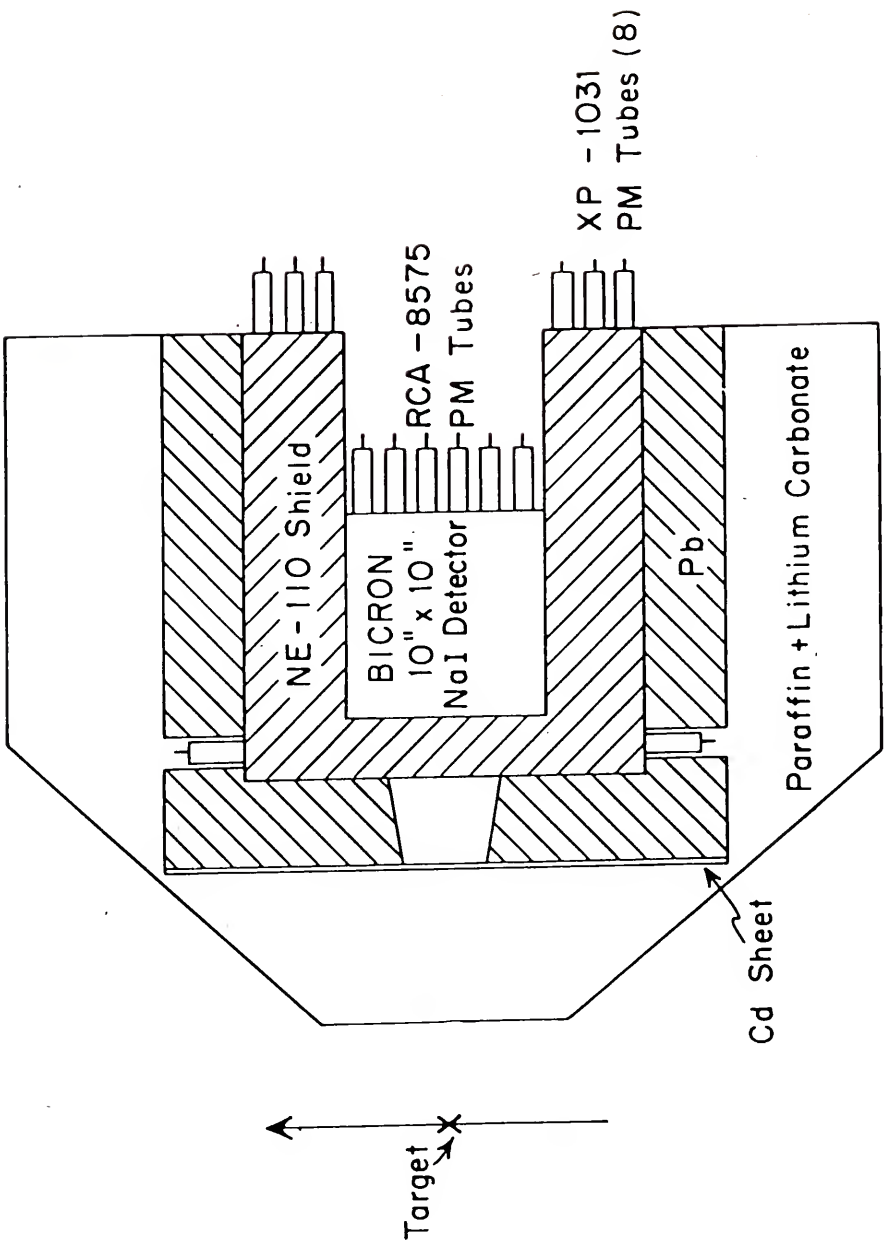
XP - 1031
PM Tubes (8)
RCA - 8575
PM Tubes
NE - 110 Shield
BICRON
10" x 10"
NaI Detector
Pb
Paraffin + Lithium Carbonate
Cd Sheet
Target

radial and angular positioning about the target location. Two radial positions of the detector were used in the experimental series. These distances placed the rear face of the NaI crystal at the positions of 82 cm and 106 cm respectively. Collimators were provided which restricted the observed solid angles to those subtended by the rear crystal face corresponding to solid angles of 7.42×10^{-2} Sr and 4.46×10^{-2} Sr respectively. Excitation curves were measured with the detector at the 82 cm distance in the interest of higher yield rates. The angular distributions were measured with the detector at the 106 position to allow the inclusion of measurements of the angles at 42^{o} and 142^{o}.

To determine the angular distribution as the laboratory angle approaches zero, additional measurements were taken for the laboratory angle of 20^{o} using a separate detector system. This system was based on a 10.2 x 17.8 cm NaI(Tl) crystal surrounded by a 22.9 x 22.9 cm NaI(Tl) annulus for active cosmic ray rejection. The experimental arrangement is shown in Figure 2.2. Passive shielding is provided by a 20.3 cm thick copper annulus and 4.4 cm of lead. A cadmium sheet was located between the lead and copper for thermal neutron absorption and the collimator was filled with paraffin loaded with lithium carbonate. The distance from the target to the crystal front face was 93.3 cm. The collimator restricts the photon flux to the

Figure 2.2 Detector Assembly for 10.2 x 17.8 cm Cylindrical NaI(Tl) Detector for Small Angle Measurement. The active and passive shielding for cosmic rays and beam associated background is shown. The beam stop shielding for measurements at $\theta_{lab} = 20^{o}$ is shown.

SMALL ANGLE DETECTOR ASSEMBLY

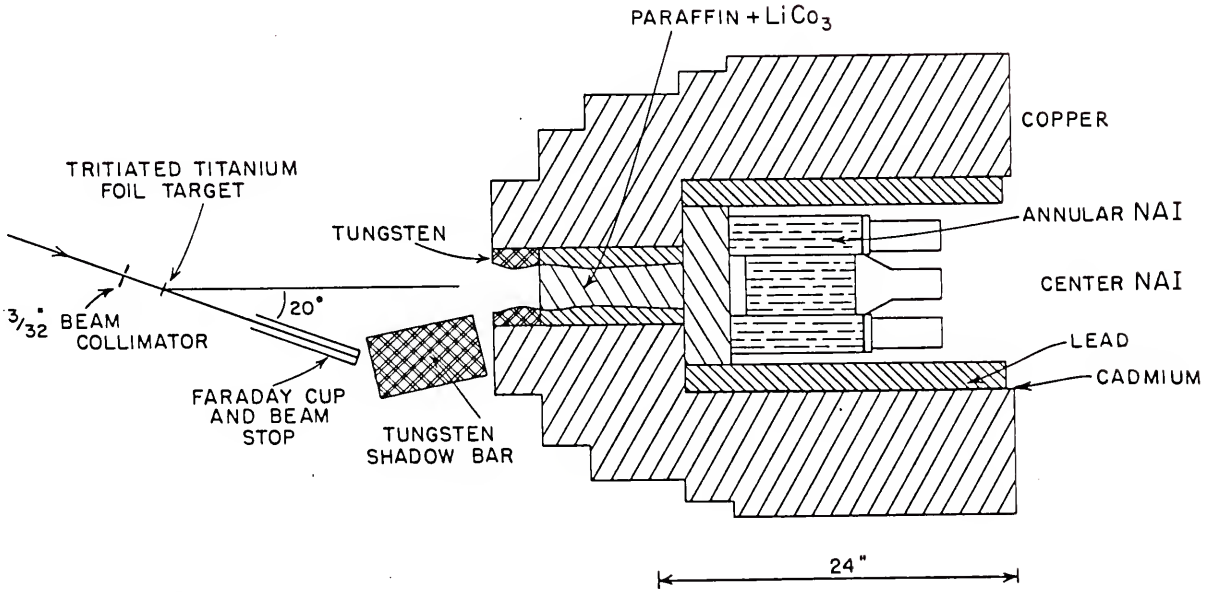

6.57×10^{-3} Sr solid angle subtended by the back face of the crystal. The entrance aperture was formed from tungsten for attenuation of fast neutrons. The remainder of the collimator was lined with lead.

Further measures to minimize the background events not associated with the target consisted of the use of a single insulated collimator close to the target and adequate shielding of the beam dump. The insulated collimator allows monitoring of the beam current striking it. This current was kept to a minimum by adjustments of the focusing of the beam transport system. The beam stop for the large crystal arrangement is located three meters beyond the target. Originally this beam stop was shielded by about 10 cm of lead and 70 cm of paraffin. The shielding was changed to about 10 cm of copper and 40 cm of lithium loaded paraffin to more effectively attenuate neutrons produced in the beam stop. For the small crystal assembly, the beam stop was located 33 cm behind the target. The shielding was provided by the copper shield of the detector itself and a tungsten shadow bar.

The electronics for the two detector systems were similar; however, the use of the NaI annular cosmic ray detector on the smaller crystal required a different electronic arrangement than the plastic shield of the 25.4 x 25.4 cm system. The electronic arrangement for the large crystal is shown in Figure 2.3 and that for the small crystal

Figure 2.3 Electronics Block Diagram for High Resolution Detector. This diagram illustrates the signal routing used to determine the coincidences between the active shield detector and the center detector. The additional electronics used to determine the number of coincidences are not shown (Weller, et al.[82]).

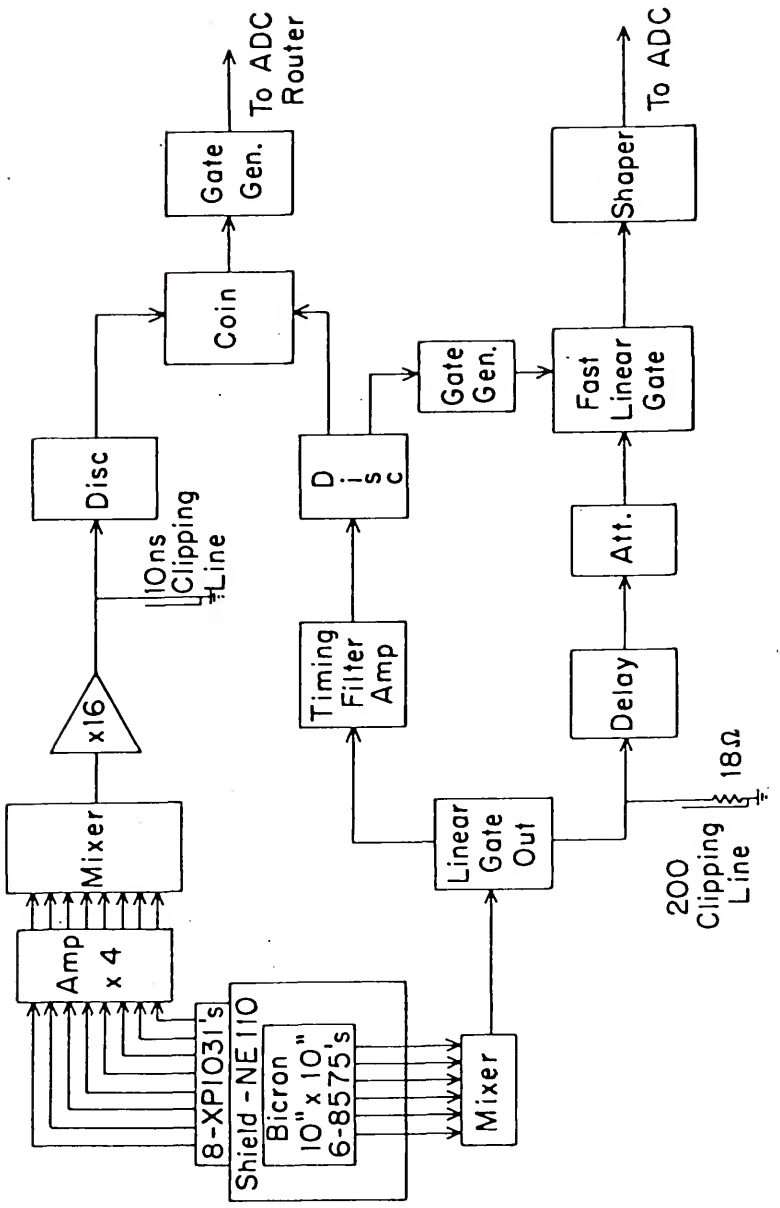
Shield - NE 110
Bicron
10" x 10"
6-8575's
8-XP1031's
Amp
x 4
Mixer
x16
Disc
110ns
Clipping
Line
Coin
Gate
Gen.
To ADC
Router
Timing
Filter
Amp
D
i
s
c
Gate
Gen.
Fast
Linear
Gate
Shaper
To ADC
Linear
Gate
Out
Delay
Att.
18Ω
200
Clipping
Line
Mixer

in Figure 2.4. Typically, the count rate due to low energy events is several orders of magnitude greater than the count rate due to events of interest. Common to both systems is the arrangement of the electronics to minimize the events due to the pileup of lower energy events. This minimization is accomplished by time-clipping the detector signals. The signal is then passed through a fast linear gate (250 ns) before processing. During the 10 μs processing time, the gate is held closed.

Further reduction of the background due to unwanted events was possible in this experimental series due to the pulsed nature of the Cyclo-Graaff beam. A time of flight requirement (TOF) was set up between a signal derived from a radio-frequency inductive pick-up loop at the Cyclotron and the gamma ray events in the center crystal. The R-F signal was used for the stop signal for a time to amplitude converter (TAC). The TAC start signal is derived from the linear signal of the NaI center crystal. The TAC was gated by the pile-up rejection circuitry to be active only for the time during which the linear gate was open. Both detectors are pulse stabilized by a calibrated light emitting diode flash into the crystal. This pulse was used to correct for slow changes in the system gain due to thermal drifts. The pulse stabilization was found to be unnecessary for the large detector system. The cosmic ray rejection was accomplished differently for the two detector systems. The

Figure 2.4 Electronics Block Diagram for Small Angle Experiment. Illustrated here are the electronics used to determine the coincidences between the active shield detector and the center detector for the yield measurement at $\theta_{lab} = 20^{o}$. The electronics associated with the pulse stabilization, accidental monitoring and beam time of flight circuits are also shown.

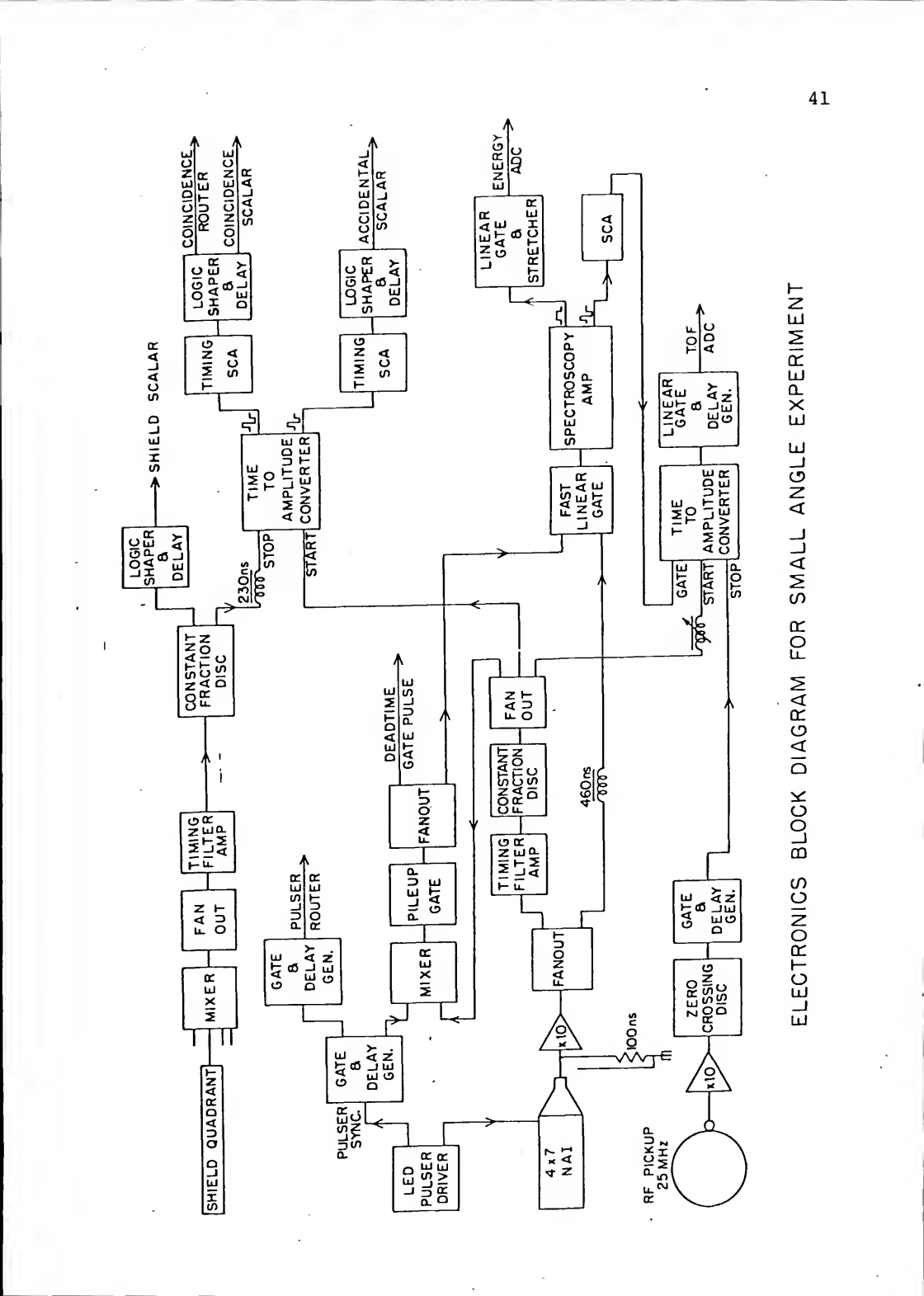

ELECTRONICS BLOCK DIAGRAM FOR SMALL ANGLE EXPERIMENT

response of the plastic scintillator is faster than that of NaI. For the large detector with the plastic shield, the shield signals were delay line clipped and timed for an overlap coincidence with the center crystal events. When a coincidence occurs, a routing signal is sent to the computer for storage of the event in a coincidence spectrum. The small crystal system utilizes the linear signal from the center crystal as the start signal for a time to amplitude converter. The shield pulses are then the stop signal for the TAC. The TAC output goes to two single channel analyzers, one of which is set to provide a signal for events occurring in the peak of the coincidence TAC spectrum. The other analyzer is set off the peak to determine the counts due to accidental coincidences. In each case the resulting signals are processed by two analog to digital converter's (ADC's) in coincidence and passed to the on-line computer. For maximum resolution, the threshold of the coincidence circuit could be set to give a coincidence for events due to annihilation γ-rays from events in the center crystal.

The information stored in the computer consisted of eight 512 channel spectra. A window light-penned on the γ-flash in the TAC spectrum separated the γ-ray events into three pairs of spectra. These pairs were stored as short time events, true data events and long time events. Each pair corresponds to center crystal events and coincidences respectively. The eighth spectrum stored was used with the

large crystal system to store the elastic proton spectrum from a 500μ silicon surface barrier detector located at a laboratory angle of 160^{o}.

The targets used in this experiment were tritiated titanium foils. The foils were 5μ thick and the activity was 6 Curies/in^2. This activity corresponds to an atomic ratio of approximately one between the tritium and the titanium. The tritium contained in the foils was determined by comparing the yield obtained by the solid state detector with the known yield of $^{3}H(p,p)^{3}H$. The measured tritium values for the two targets used were 0.14 mg/cm^2 and 0.11 mg/cm^2. The error in these concentrations is determined by the uncertainty in the experimental geometry and is estimated to be 10%. The errors associated with the statistics, the $^{3}H(p,p)^{3}H$ cross section and the beam charge measurement combined contribute about 1% to this error.

Experimental Data

The experimental data were taken in four series. The first series consisted of a set of excitation curves which were utilized to determine the experimental asymmetry of the angular distribution. The second series consisted of angular distributions measured at eight angles between 42^{o} and 142^{o}. These measurements were extended in the third series to include a measurement at an angle of 20^{o}. The fourth series was an extension of the excitation curve data to lower

energies than covered in the first series. This data was then analyzed to determine the effects due to contributions from the electric quadrupole interaction.

In the first series, the excitation curves were measured for laboratory angles that transform approximately to the center of mass angles of 55^{o}, 93^{o}, and 125^{o} (Figures 2.5, 2.6). The measurement was taken in 500 keV steps over the energy range from 17-30 MeV. The resulting cross sections are shown in Table 2.1. The center of mass angle in the forward direction ($\theta_f \simeq 55^{o}$) and in the backward direction ($\theta_B \simeq 125^{o}$) were chosen to be approximately the zeros of the second order Legendre polynomial P_2 (cos θ). This condition on θ_f and θ_B requires that $\theta_B = 180-\theta_f$ which yields the following results for the Legendre polynomials:

$$\begin{aligned} P_1 (\cos \theta_B) &= -P_1(\cos \theta_f) \\ P_2 (\cos \theta_B) &= P_2(\cos \theta_f) = 0 \\ P_3 (\cos \theta_B) &= -P_3(\cos \theta_f) \\ P_4 (\cos \theta_B) &= P_4(\cos \theta_f) \end{aligned} \qquad (2.1)$$

The observed yield as a function of angle can be written as an expansion of Legendre polynomials,

$$Y(\theta) = A_o(1 + \sum_{k=1} a_k P_k(\cos \theta)).$$

Figure 2.5 $^{3}H(p,\gamma)^{4}He$ Center of Mass Cross Section for $\theta_{lab} = 90^{o}$. The data from this series of experiments is shown as the solid dots. The error bars represent the statistical error associated with the data points. The data is plotted both as a function of the laboratory energy of the incident proton and the center of mass energy of the emitted gamma ray. The experimental cross section reported by Meyerhof, et al.[13] is included as the open squares. The solid curve is a least squares fit of the data in the proton energy range from 5 to 30.5 MeV to a cubic polynomial. The cross section was obtained by normalizing to the data of Meyerhof.[13] The measured target thickness, solid angle and collected charge was combined with the normalization to obtain the detector efficiency. The value of 27 ± 3% obtained is consistent with the efficiency 26 ± 6% reported by Weller, et al.[82]

Figure 2.6 $^{3}H(p,\gamma)^{4}He$ Center of Mass Cross Sections for $\theta_{cm} = 55^{o}$ and 125^{o}. The experimental data is shown as the solid dots with the error bars indicating the associated statistical error. The data is plotted both as a function of the laboratory energy of the incident proton and the center of mass energy of the emitted gamma ray. The solid lines are fits to the data in terms of the model discussed in Chapter III.

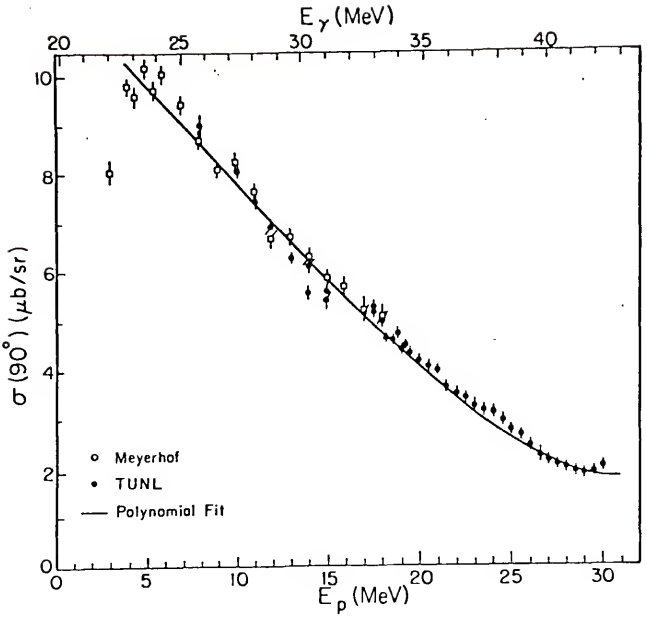
E γ (MeV)
20
25
30
35
40
10
8
6
4
2
0
σ (90°) (μb/sr)
o Meyerhof
• TUNL
— Polynomial Fit
0
5
10
15
20
25
30
E p (MeV)

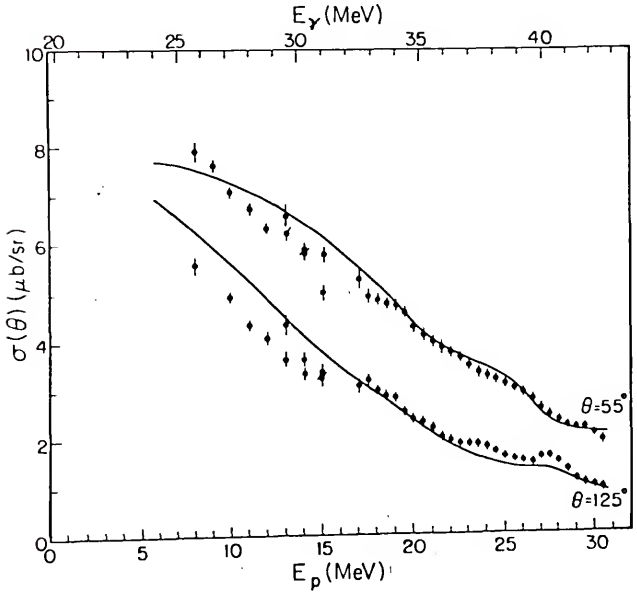
E γ (MeV)
20
25
30
35
40
10
8
6
4
2
0
σ (θ) (μb/sr)
θ=55°
θ=125°
0
5
10
15
20
25
30
E p (MeV)

Table 2.1

Measured Differential Cross Sections in the Center of Mass

Proton Beam Energy (MeV)	Center of Target	$E_{\gamma cm}$ (MeV)	$\theta_{lab}=53.5^{o}$		$\theta_{lab}=90^{o}$		$\theta_{lab}=123.5^{o}$	
			$\sigma_{p,\gamma}(\theta)\mu b$	$\sigma_{\gamma,p}(\theta)\mu b$	$\sigma_{p,\gamma}(\theta)\mu b$	$\sigma_{\gamma,p}(\theta)\mu b$	$\sigma_{p,\gamma}(\theta)\mu b$	$\sigma_{\gamma,p}(\theta)\mu b$
8.0	7.96	25.7	7.90 ± .22	252.8 ± 5.6	8.96 ± .27	228.9 ± 6.9	5.58 ± .18	142.6 ± 4.6
9.0	8.96	26.5	7.62 ± .13	206.9 ± 3.5				
10.0	9.96	27.2	7.08 ± .11	202.1 ± 3.1	8.19 ± .24	233.8 ± 8.2	4.93 ± .10	140.8 ± 2.9
11.0	10.97	27.9	6.75 ± .11	200.9 ± 3.3	7.47 ± .22	222.3 ± 6.5	4.37 ± .09	130.1 ± 2.7
12.0	11.97	28.7	6.36 ± .10	196.0 ± 3.2	6.95 ± .19	214.1 ± 5.9	4.07 ± .09	125.4 ± 2.8
13.0	12.97	29.4	6.23 ± .10	197.6 ± 3.2	6.29 ± .18	199.5 ± 5.7	3.68 ± .08	116.7 ± 2.5
14.0	13.97	30.2	5.85 ± .10	190.2 ± 3.2	5.63 ± .17	183.0 ± 5.5	3.37 ± .08	109.6 ± 4.0
15.0	14.97	31.3	5.61 ± .14	186.1 ± 4.6	5.43 ± .16	180.2 ± 5.3	3.39 ± .13	112.5 ± 4.3

Table 2.1 (continued)

			$\theta_{lab}=53^{o}$		$\theta_{lab}=90^{o}$		$\theta_{lab}=120^{o}$	
17.0	16.98	32.4	5.42 ± .14	185.6 ± 4.8	5.24 ± .29	179.5 ± 9.9	3.17 ± .18	108.5 ± 6.2
17.5	17.48	32.8	5.07 ± .13	174.8 ± 4.5	5.28 ± .11	182.0 ± 3.8	3.65 ± .19	125.8 ± 6.5
18.0	17.98	33.1	5.12 ± .13	177.5 ± 4.5	5.01 ± .08	173.7 ± 2.8	2.87 ± .17	99.5 ± 5.9
18.5	18.48	33.5	4.92 ± .13	171.5 ± 4.5	4.61 ± .09	160.7 ± 3.1	2.97 ± .17	103.5 ± 5.9
19.0	18.98	33.9	5.02 ± .13	175.8 ± 4.5	4.43 ± .07	155.1 ± 2.4	3.12 ± .18	109.3 ± 6.3
19.5	19.48	34.2	4.84 ± .12	170.2 ± 4.2	4.35 ± .09	152.0 ± 3.2	2.50 ± .16	87.9 ± 5.6
20.0	19.98	34.6	4.43 ± .11	156.4 ± 3.9	4.18 ± .07	147.6 ± 2.5	2.41 ± .13	85.1 ± 4.6
20.5	20.48	35.0	4.28 ± .10	151.6 ± 3.5	4.07 ± .09	144.2 ± 3.2	2.56 ± .13	90.7 ± 4.6

Table 2.1 (continued)

			$\theta_{lab}=53^{o}$		$\theta_{lab}=90^{o}$		$\theta_{lab}=123^{o}$	
21.0	20.98	35.4	4.20 ± .10	149.3 ± 3.6	3.98 ± .07	141.4 ± 2.5	2.15 ± .13	76.4 ± 4.6
21.5	21.48	35.7	4.03 ± .10	143.6 ± 3.6	4.04 ± .09	144.8 ± 3.2	2.22 ± .13	79.1 ± 4.6
22.0	21.98	36.1	3.91 ± .10	139.7 ± 3.6	3.76 ± .07	134.3 ± 2.5	1.93 ± .12	69.0 ± 4.3
22.5	22.48	36.5	3.81 ± .10	136.4 ± 3.6	3.60 ± .08	128.9 ± 2.9	2.08 ± .12	74.5 ± 4.3
23.0	22.98	36.8	3.61 ± .09	129.5 ± 3.2	3.56 ± .07	127.7 ± 2.5	1.86 ± .12	66.7 ± 4.3
23.5	23.48	37.2	3.47 ± .09	124.7 ± 3.2	3.52 ± .07	126.5 ± 2.5	2.10 ± .13	75.5 ± 4.7

Table 2.1 (continued)

			$\theta_{lab}=53.5^{o}$		$\theta_{lab}=90^{o}$		$\theta_{lab}=123.5^{o}$	
24.0	23.98	37.6	3.42 ± .08	123.1 ± 2.9	3.21 ± .05	115.5 ± 1.8	1.76 ± .10	63.3 ± 3.6
24.5	24.48	37.9	3.34 ± .08	120.3 ± 2.9	3.34 ± .07	120.3 ± 2.5	1.81 ± .10	65.2 ± 3.6
25.0	24.98	38.3	3.22 ± .07	116.1 ± 2.5	3.31 ± .05	119.4 ± 1.8	1.72 ± .09	62.0 ± 3.2
25.5	25.48	38.7	3.14 ± .07	113.3 ± 2.5	3.22 ± .06	116.2 ± 2.2	1.49 ± .09	53.8 ± 3.2
26.0	25.98	39.0	3.06 ± .07	110.5 ± .06	3.09 ± .06	111.5 ± 2.2	1.74 ± .10	62.8 ± 3.6
26.5	26.48	39.4	2.88 ± .07	104.0 ± 2.5	3.23 ± .05	116.6 ± 1.8	1.33 ± .08	48.0 ± 2.9
27.0	26.98	39.8	2.68 ± .07	96.8 ± 2.5	3.03 ± .05	109.4 ± 1.8	1.79 ± .07	64.6 ± 2.5
27.5	27.48	40.2	2.55 ± .07	92.1 ± 2.5	3.08 ± .06	111.2 ± 2.2	1.70 ± .07	61.4 ± 2.5
28.0	27.98	40.5	2.45 ± .06	88.5 ± 2.2	2.82 ± .05	101.8 ± .05	1.55 ± .06	56.0 ± 2.2
28.5	28.48	40.9	2.33 ± .06	84.1 ± 2.2	2.71 ± .06	97.9 ± 2.2	1.45 ± .06	52.4 ± 2.2
29.0	28.98	41.3	2.29 ± .06	82.7 ± 2.2	2.03 ± .10	98.2 ± 1.8	1.06 ± .05	38.2 ± 1.8
29.5	29.48	41.6	2.28 ± .06	82.2 ± 2.2	1.88 ± .09	102.4 ± 2.2	1.13 ± .05	40.7 ± 1.8
30.0	29.98	42.0	2.15 ± .06	77.5 ± 2.2	2.10 ± .10		1.07 ± .05	38.5 ± 1.8
30.5	30.48	42.4	2.02 ± .10	72.7 ± 3.5			.99 ± .05	35.6 ± 1.8

Under the assumption that multipolarities of L > 2 contribute negligibly to the cross section, the sum of the yields for the angles θ_f and θ_B reduces to

$$Y(\theta_f) + Y(\theta_B) = 2A_o(1+a_4P_4(\cos\theta_f)). \tag{2.2}$$

where a_o and a_4 are defined in equation (1.4). The difference between the yields is then

$$\begin{aligned} Y(\theta_f)-Y(\theta_B) &= A_o(a_1P_1(\cos\theta_f)+a_3P_3(\cos\theta_f)-a_1P_1(\cos\theta_B) \\ &\quad -a_3P_3(\cos\theta_B)) \\ &= 2A_o(a_1P_1(\cos\theta_f)+a_3P_3(\cos\theta_f)). \end{aligned} \tag{2.3}$$

Therefore, assuming the condition $a_4P_4(\cos\theta_f)<<1$, which should be expected if the E2 intensity is small compared to the E1 intensity, the total cross section is given by

$$\sigma_t = 4\pi A_o \simeq 2\pi(Y(\theta_f)+Y(\theta_B)) \tag{2.4}$$

and

$$A_o \simeq \tfrac{1}{2}\,(Y(\theta_f)+Y(\theta_B)). \tag{2.5}$$

Under these conditions, the experimental asymmetry in terms of the yields $Y(\theta_f)$ and $Y(\theta_B)$ is equivalent to that defined in terms of the coefficients of the Legendre expansion of the angular distribution (Figure 2.7). This equivalence is shown by the following relations:

$$\begin{aligned} a_s &= \frac{Y(\theta_f) - Y(\theta_B)}{P_1(\cos\theta_f)(Y(\theta_f)+Y(\theta_B))} = \frac{2A_o(a_1P_1(\cos\theta_f)+a_3P_3(\cos\theta_f))}{P_1(\cos\theta_f)(2A_o(1+a_4P_4(\cos\theta_f))} \\ &\simeq a_1 + \frac{P_3(\cos\theta_f)a_3}{P_1(\cos\theta_f)}\ ,\ a_4P_4(\cos\theta_f)<<1. \end{aligned} \tag{2.6}$$

Figure 2.7 $^{3}H(p,\gamma)^{4}He$ Angular Distributions. The experimental data is shown as the solid dots with the error bars indicating the associated statistical error. The solid lines are least squares fits to the data in terms of the Legendre Polynomials as discussed in Chapter III. The measured values for the cross sections are included in Appendix B.

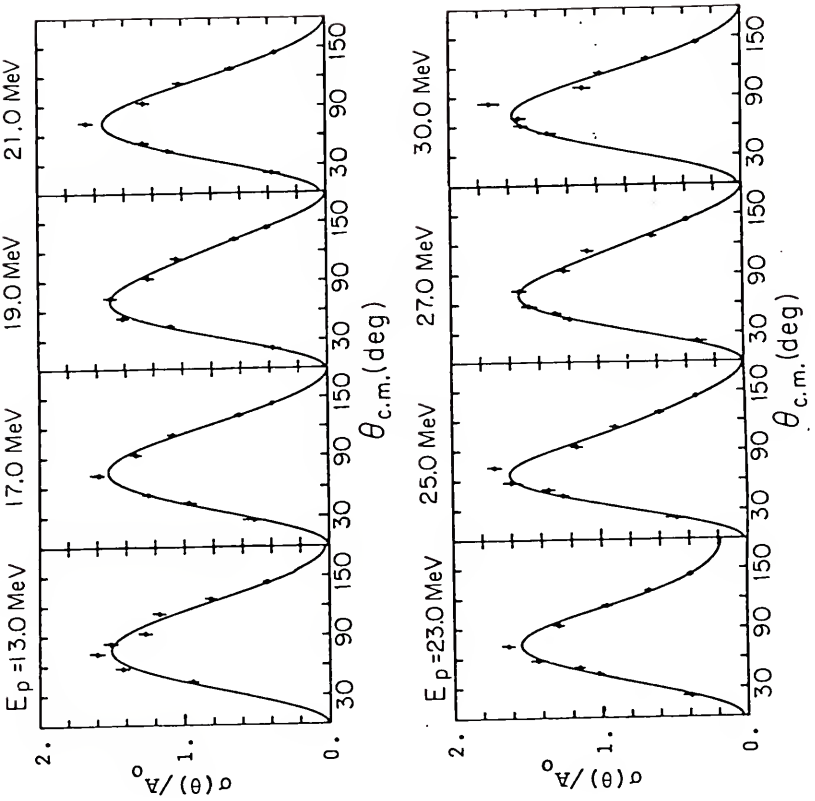
Ep =13.0 MeV
17.0 MeV
19.0 MeV
21.0 MeV
Ep =23.0 MeV
25.0 MeV
27.0 MeV
30.0 MeV
σ(θ)/Ao
θc.m.(deg)
0.
1.
2.
30
90
150

As will be shown in Chapter III, the measured asymmetry and the measured cross section can be used to obtain an experimental E2 cross section.

The E1 cross section is obtained by observing that the terms of the multipole expansion (equation 1.5) for multipolarities up to L = 4 reduce to $\frac{d\sigma}{d\Omega} = B\ (\alpha + 1)$ at $\theta_{cm} = 90^{o}$.

Therefore, taking $\alpha << 1$ (no spin-flip or magnetic dipole radiation) the yield at this angle is the E1 cross section.[13,19,33] The angle measured was $\theta_{lab} = 90^{o}$ so that the results could be readily compared with those of previous experimenters.[13,56]

A second experimental series was conducted to confirm the energy behavior of the E2 cross section and to provide a direct measurement of the E2 amplitude. This series consisted of a set of angular distribution measurements taken every 2 MeV between 17 and 27 MeV incident proton energy, and included angular distributions measured for proton energies of 13 and 30 MeV. For each angular distribution, yields were measured for a minimum of seven angles in the range 42^{o}-142^{o} covered by the detector. Additional angles were included as needed to define the shape of the peak and the slope of the sides of the angular distribution. The minimum number of measurement points was chosen so that the number of degrees of freedom associated with a Legendre polynomial least squares fit to four

coefficients is greater than zero. The amount of charge collected was varied so that a minimum of 200 counts was observed for the 142^{o} measurement. The yield was larger for all other angles observed (Figure 2.7).

The third series of measurements was conducted using the 10.2 x 17.8 cm NaI detector. The purpose of this experimental series was to determine the shape of the angular distribution as the angle approaches zero. Measurements were made every 2 MeV in the proton energy range $17 \leq E_p \leq 27$ MeV. Yields were measured for three laboratory angles including 20^{o}, 90^{o} and an intermediate angle corresponding to an angle at each energy for which the yield was measured in the second series. These measurements were normalized to the data of the second series, and an effective yield for the 25.4 x 25.4 cm detector at the laboratory angle of 20^{o} was obtained. This yield was incorporated into the angular distributions used to determine the Legendre expansion coefficients.

The fourth series of measurements extended the asymmetry data to lower energy. The TUNL FN tandem was used to measure the fore-aft asymmetry every 1 MeV in the proton energy range from $8 \leq E_p \leq 15$ MeV. This information was obtained for comparison with the published results of earlier experimenters.[13]

CHAPTER III
DATA ANALYSIS

Kinematics

The kinematics of the reaction $^{3}H(p,\gamma)^{4}He$ for proton energies above 10 MeV are subject to relativistic corrections. Therefore, the kinematics were explicitly treated according to special relativity following the treatment by J. J. Jackson.[84] The reaction coordinates in the laboratory and center of momentum frames are shown in Figure 3.1.

Laboratory Center of Momentum

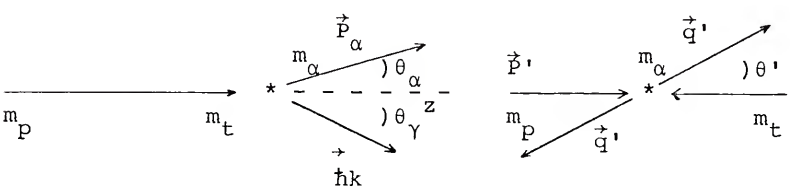

Figure 3.1 Laboratory and Center of Momentum Coordinates

The conservation equation for the square of the four momentum of the alpha particle in its rest frame and in the laboratory system is

$$(0, j/_c\, m_\alpha c^2)^2 = (\sqrt{\gamma^2_p - 1}\; m_p c\hat{k} - \hbar\vec{k},\; j/_c\,(\gamma_p m_p c^2 + m_t c^2 - E_\gamma))^2 \quad (3.1)$$

where γ_p is the Lorentz transformation parameter. For the proton in the laboratory, this parameter is $\gamma_p = 1/\sqrt{1-v_p^2/c^2}$. Solving the conservation equation for the laboratory gamma ray energy as a function of laboratory angle gives

$$E_\gamma = \frac{(E')^2 - m_\alpha^2 c^4}{2(\gamma_p m_p c^2 + m_t c^2 - \sqrt{\gamma_p^2 - 1}\, m_p c^2 \cos\theta_\gamma)} \tag{3.2}$$

where the energy

$$E' = (m_p^2 c^4 + m_t^2 c^4 + 2\gamma_p m_p c^2 m_t c^2)^{\frac{1}{2}} \tag{3.3}$$

is the total energy in the center of mass system.

The gamma ray energy in the center of mass is

$$E'_\gamma = \frac{(E')^2 - m_\alpha^2 c^4}{2E'} \,. \tag{3.4}$$

The excitation energy of the compound nucleus is found by subtracting the alpha particle rest energy from the total center of mass energy

$$E_x = E' - m_\alpha c^2 \tag{3.5}$$

The relationship between the angle in the center of momentum and in the laboratory is given by

$$\theta' = \tan^{-1}\left(\frac{\sin\theta_\gamma}{\gamma_{cm}(\cos\theta_\gamma - \beta)}\right) \text{ where } \beta = \frac{\sqrt{\gamma_p^2 - 1}}{\gamma_p^2} \,, \tag{3.6}$$

where the Lorentz transformation parameter for the center of momentum γ_{cm} is related to the total laboratory energy and

the total energy of the compound nucleus by

$$\gamma_{cm} = \frac{\gamma_p m_p c^2 + m_t c^2}{E'} \tag{3.7}$$

These relations were incorporated in the computer programs used for data analysis.

The relationship between the measured cross section in the laboratory reference frame and that of the center of momentum reference frame is also necessary for comparison of the experiment to theory. This relation can be obtained from the equality of the yield in the two frames following Marion.[85] This equality is

$$\sigma_{lab}(\theta_\gamma)d\Omega = \sigma_{cm}(\theta')d\Omega'. \tag{3.8}$$

Using the kinematic relations between θ_γ and θ' with the definitions of the solid angle increments, which are $d\Omega = 2\pi \sin\theta_\gamma d\theta_\gamma$ and $d\Omega' = 2\pi \sin\theta' d\theta'$, the relation between the two differential cross sections is found to be as follows:

$$\sigma_{lab}(\theta_\gamma) = \sigma_{cm}(\theta') \frac{\sin^3\theta'}{\sin\theta_\gamma} \left(\frac{\cos\theta'\cos\theta_\gamma}{\sin\theta'\sin\theta_\gamma} + \gamma_{cm}\right). \tag{3.9}$$

This form of the relation between the two frames was convenient to use as the analysis programs calculated θ' and γ_{cm} for measured gamma ray angle θ_γ.

Excitation Curve Analysis

Assuming only E1 and E2 radiation with the additional assumption that the E1 and E2 spin-flip terms are negligible, the cross section may be written in terms of the spherical harmonics Y_{11} and Y_{21}. The interaction is modeled by assuming that it consists of direct and resonance terms. The center of mass cross section expression is

$$\frac{d\sigma_{\gamma,p}(\theta)}{d\Omega} = |\varepsilon_1 D_1 e^{i\delta_1} Y_{11} + (\varepsilon_2 D_2 e^{i\delta_2} + R_1 e^{i(\Phi_1+\eta_1)} + R_2 e^{i(\Phi_2+\eta_2)}) Y_{21}|^2 \quad . \tag{3.10}$$

[41]

This expression for the cross section implicitly includes the relations $a_3 = -a_1$ and $1 + a_2 + a_4 = 0$ between the coefficients in the Legendre expansion. The first term of the cross section is due to a direct E1 interaction. The second term is due to a direct E2 interaction, The factors ε_1 and ε_2 are the kinematic effective charges.[86] The third and fourth terms are resolved Breit Wigner resonances centered around energies E_1 and E_2 respectively. Each term of this expression will be examined further in the following paragraphs.

The expressions for the resonance terms in the center of mass are

$$R_1 = \frac{g_1 (E'_\gamma)^{3/2} P_p^{1/2}}{((E'_\gamma - E)^2 + \Gamma_1^2/4)^{1/2}} \tag{3.11}$$

and

$$R_2 = \frac{g_2 (E'_\gamma)^{3/2} P_p^{1/2}}{((E'_\gamma - E)^2 + \Gamma_2^2/4)^{1/2}} \tag{3.12}$$

The energy dependence of the resonance partial widths is explicitly included in these expressions where P_p is the proton penetrability calculated by the method of B. Buck, et al.[87] and

$$(E'_\gamma)^{3/2} \propto \left(\frac{(E'_\gamma)^{2L+1}}{k^2}\right)^{1/2} \propto \frac{\Gamma_\gamma^{1/2}}{E'_\gamma}$$

describes the energy dependence of the transition amplitude (Γ_γ) of a L = 2 multipole. The resonance strength for the gamma ray resonant absorption is then

$$\frac{\pi \hbar^2 c^2 (2L+1)}{(E'_\gamma)^2} \Gamma_\gamma \Gamma_p = \frac{4\pi g^2 (E'_\gamma)^{2L+1} P_p}{(E'_\gamma)^2} \tag{3.13}$$

The energy dependence of the total width of the resonance is included by using the proton and neutron penetrabilities and their respective reduced widths, i.e.

$$\Gamma = \Gamma_n + \Gamma_p = 2\gamma_n^2 P_n + 2\gamma_p^2 P_p \ . \tag{3.14}$$

The deuteron and gamma partial widths are assumed to be negligible with respect to the neutron and proton partial widths. The reduced widths are solutions to the equations

$$\Gamma(E) = 2\gamma_n^2 P_n(E) + 2\gamma_p^2 P_p(E) \tag{3.15}$$

and

$$\gamma_n^2 = \gamma_p^2$$

for the resonance centered about the energy E. The neutron and proton contributions are here assumed to differ only by coulomb effects. The phase Φ in each case is the resonance phase, given by

$$\Phi_i = \tan^{-1} \left(\frac{E - E_i}{\Gamma_i/2}\right) \tag{3.16}$$

The phases η_1 and η_2 account for the relative phases between the resonances and the direct terms.

The functional form for the direct terms was taken from the analysis of Flowers and Mandl.[88] They assume gaussian type wave functions and obtain relations of the form

$$D_1 e^{i\delta_1} = \alpha_1 (E'_\gamma)^{1/2} E_p^{3/4} e^{-bE_p} e^{i\delta_1} \tag{3.17}$$

and

$$D_2 e^{i\delta_2} = \alpha_2 (E'_\gamma)^{3/2} E_p^{5/4} e^{-bE_p} e^{i\delta_2} . \tag{3.18}$$

The gaussian wave functions parameters are chosen to fit the ^{4}He rms. radius of 1.61 fm. given by electron scattering giving $\alpha_1 = .101$ $(mb/MeV^{5/2})^{1/2}$, $\alpha_2 = 5.13 \times 10^{-5}$ $(mb/MeV^{11/2})^{1/2}$ and $b = .043$ MeV^{-1}.[41] For comparison to the experimental data, the direct E1 term was replaced with an empirical function and the strength of the E2 term, α_2, was allowed to vary. The phases δ_1 and δ_2 were varied to obtain the relative phase between the direct E1 and E2 terms that best fit the data.

The above expression for the differential cross section is in the form of products of spherical harmonics. These products are expanded in terms of single spherical harmonics. The product expansion is

$$Y_{\ell m}(\Omega)Y_{\ell' m'}(\Omega) = (-1)^m \sum_{L=|\ell-\ell'|}^{\ell+\ell'} \sum_{M=-L}^{L} \left[\frac{(2\ell+1)(2\ell'+1)}{4\pi(2L+1)}\right]^{1/2} C^{000}_{\ell'\ell L} C^{m'mM}_{\ell'\ell L} Y_{LM}(\theta,\Phi), \quad (3.19)$$

where the Clebsh-Gordon coefficient $C^{m'mM}_{\ell'\ell L}$ is zero for $M \neq m'-m$. The resulting expansion is in terms of the Y_{L0} functions alone. The functions Y_{L0} are simply related to the Legendre polynomials by the function

$$Y_{L0}(\theta,\Phi) = \frac{\sqrt{2L+1}}{4\pi} P_L(\cos\theta) \quad (3.20)$$

Collecting the terms of the polynomials and comparing with the Legendre expansion of the angular distribution allows identification of the expansion coefficients in terms of the

direct and resonance contributions of the model. In order to make this identification the following three definitions are made:

$$B_o = (\varepsilon_1 D_1)^2$$

$$B_1 = [2\varepsilon_1 D_1 \varepsilon_2 D_2 \cos(\delta_1-\delta_2) - 2\varepsilon_1 D_1 (R_1 \cos(\Phi_1+\eta_1-\delta_1) + R_2 \cos(\Phi_2+\eta_2-\delta_1))]$$

$$B_2 = [(\varepsilon_2 D_2)^2 - 2\varepsilon_2 D_2 (R_1 \cos(\Phi_1+\eta_1-\delta_2) + R_2 \cos(\Phi_2+\eta_2-\delta_2)) + R_1^2$$

$$+ 2R_1 R_2 \cos(\Phi_1+\eta_1-\Phi_2-\eta_2) + R_2^2]. \qquad (3.21)$$

In these definitions B_o appears in terms of only E1 amplitudes, B_1 appears in terms of products of E1 and E2 amplitudes, and B_2 appears in terms of E2 amplitudes only. The coefficients of the cross section expansion may then be written as follows:

$$A_o = \frac{1}{4\pi}(B_o+B_2),\quad A_o a_1 = \frac{3}{4\pi\sqrt{5}} B_1,\quad A_o a_2 = \frac{1}{4\pi}(-B_o+\frac{5}{7}B_2),$$

$$A_o a_3 = -A_o a_1,\quad A_o a_4 = \frac{-12}{7(4\pi)}B_2 \ . \qquad (3.22)$$

In this form the E1 and E2 contributions are explicitly included.

The Legendre expansion gives the differential cross section as a function of angle θ in the limit of infinitesmal solid angle; however, the actual detector solid angle is finite. In order to compare the model to experiment, it is therefore necessary to transform to finite geometry. This

transformation introduces geometric correction factors Q_i (Ferguson [89]) into the expansion. The resulting expression for the experimental cross section is

$$\frac{\Delta_{\gamma,p}\sigma(\theta)}{\Delta\Omega} = A_o(Q_o + a_1Q_1P_1(\cos\theta) + a_2Q_2P_2(\cos\theta) + a_3Q_3P_3(\cos\theta) + a_4Q_4P_4(\cos\theta)) \quad (3.23)$$

The yield from the $^3H(p,\gamma)^4He$ reaction is converted to the photonuclear reaction $^4He(\gamma,p)^3H$ by the principle of detailed balance. The relationship between the cross sections is given by

$$\sigma_{\gamma,p}(\theta) = \frac{1}{2}\left(\frac{(2I(^1H)+1)(2I(^3H)+1)}{(2I(^4He)+1)}\right)\left(\frac{2m_pc^2E_p}{E_\gamma^2}\right)\sigma_{p,\gamma}(\theta). \quad (3.24)$$ [90]

where I(A) is the nuclear spin of nucleus A.

Using these relations, a computer program was developed which plotted the model cross sections against the measured cross sections as a function of energy and angle. The model parameters for the curves that best represented the plotted experimental data were used to obtain the resonance parameters and the integrated strength of the various components of the model. These results are presented at the end of this Chapter.

Angular Distributions

The angular distribution data were measured in an attempt to obtain a direct measurement of the E2 strength through a determination of the coefficient a_4. The magnitude of the cross section for $\theta = 0^\circ, 180^\circ$ also provides a determination of the contribution of spin-flip interactions to the cross section. The experimental data are fit by linear least squares to the first four terms of the Legendre cross section expansion for finite geometry as discussed in the previous section. For some measurements, the resulting fits were negative for $\theta = 0^\circ, 180^\circ$. A non-linear least squares search with the additional requirement that the cross section be positive was then used to obtain the values for the coefficients A_o, a_1, a_2, a_3, and a_4. The error associated with each coefficient is then obtained from the curvature of the Chi-square space.

The assumption that the E1 and E2 spin flip is negligible is tested by the angular distributions. The truncated Legendre expansion reduces to

$$\frac{d\sigma}{d\Omega}(\theta) = A_o(1+a_1+a_2+a_3+a_4) \qquad (3.25)$$

at $\theta = 0^\circ$ and

$$\frac{d\sigma}{d\Omega}(\theta) = A_o(1-a_1+a_2-a_3+a_4)$$

at $\theta = 180^\circ$. The cross section is equal at these two angles for $a_3 = -a_1$ and zero if in addition $1+a_2+a_4 = 0$. Assuming only E1

and E2 radiation, the coefficients $A_o a_1$ and $A_o a_3$ can be written in terms of the complex vectors $|j_\alpha j_\beta J>$ for total angular momentum ($\vec{j}\cdot\vec{j}$) coupling where $\vec{j}_\alpha = \vec{\ell}_\alpha + \vec{s}_\alpha$ is the total angular momentum of the incident particle, $\vec{j}_\beta = \vec{s}_\beta$ is the total angular momentum of the target and $\vec{J} = \vec{j}_\alpha + \vec{j}_\beta$ is the total angular momentum of the system. The nuclear spins are $\vec{s}_\alpha$ and $\vec{s}_\beta$ of the projectile and target respectively, while $\vec{\ell}_\alpha$ is the orbital angular momentum. The R matrix elements ($<I\,\mathcal{L}\,J||T||j_\alpha j_\beta J>$) for radiation of multipolarity $\mathcal{L}$ and compound nucleus of ground state spin I = 0 are the following for E1 and E2 radiation:

$$<011||T||\tfrac{1}{2}\tfrac{1}{2}1> = P_{\frac{1}{2}} e^{i^1\Phi_{\frac{1}{2}}},\quad <011||T||\tfrac{3}{2}\tfrac{1}{2}1> = P_{\frac{3}{2}}\, e^{i\Phi_{\frac{3}{2}}}$$
$$<022||T||\tfrac{3}{2}\tfrac{1}{2}2> = d_{\frac{3}{2}} e^{i^2\Phi_{\frac{3}{2}}},\quad <022||T||\tfrac{5}{2}\tfrac{1}{2}2> = d_{\frac{5}{2}} e^{i^2\Phi_{\frac{5}{2}}}. \tag{3.27}$$

The resulting expression for the coefficients are as follows:

$$\begin{aligned} A_o a_1 = \frac{3}{4}\{&\sqrt{10}\ \mathrm{Re}(P_{\frac{1}{2}} d_{\frac{3}{2}}\ e^{i(^2\Phi_{\frac{3}{2}} - {}^1\Phi_{\frac{1}{2}})}) \\ &-\frac{\sqrt{5}}{5}\ \mathrm{Re}(P_{\frac{3}{2}} d_{\frac{3}{2}}\ e^{i(^2\Phi_{\frac{3}{2}} - {}^1\Phi_{\frac{3}{2}})}) \\ &+\frac{3\sqrt{30}}{5}\ \mathrm{Re}(P_{\frac{3}{2}} d_{\frac{5}{2}}\ e^{i(^2\Phi_{\frac{5}{2}} - {}^1\Phi_{\frac{3}{2}})})\} \end{aligned} \tag{3.28}$$

$$A_o a_3 = \frac{1}{2}\{\sqrt{15}\ \mathrm{Re}(P_{1/2} d_{3/2}\, e^{i(^2\Phi_{3/2} - {}^1\Phi_{1/2})})$$

$$+\frac{9\sqrt{5}}{5}\ \mathrm{Re}(P_{3/2} d_{3/2}\, e^{i(^1\Phi_{3/2} - {}^2\Phi_{3/2})}) \qquad (3.29)$$

$$-\frac{2\sqrt{30}}{5}\ \mathrm{Re}(P_{3/2} d_{5/2} e^{i(^1\Phi_{3/2} - {}^2\Phi_{5/2})})\}$$

The relationship $a_3 = -a_1$ can be obtained from these equations by imposing the following conditions on the phases

$$^1\Phi_{3/2} = {}^1\Phi_{1/2} + n\pi$$

$$n = 0,2,4, \ldots \qquad (3.30)$$

$$^2\Phi_{5/2} = {}^2\Phi_{3/2} + n\pi$$

With these conditions there are two possible classes of solutions to equations 3.28 and 3.29 that lead to the result $a_3 = -a_1$. One class is obtained when the ratio between the magnitudes $d_{3/2}$ and $d_{5/2}$ equals $-\sqrt{6}/3$ in which case the ratio between the magnitudes $P_{1/2}$ and $P_{3/2}$ is indeterminate. The other possible class of solutions is obtained when the ratio between the magnitudes $P_{1/2}$ and $P_{3/2}$ equals $-\sqrt{2}/2$ in which case the ratio of the magnitudes $d_{3/2}$ and $d_{5/2}$ is indeterminate.

Alternatively the system may be described in terms of the $(\vec{L}\cdot\vec{S})$ coupling vectors ($|\ell_\alpha S_\alpha \ell_\beta S_\beta LSJ>$). The total angular momentum is $\vec{L} = \vec{\ell}_\alpha + \vec{\ell}_\beta$ and the total spin is $\vec{S} = \vec{S}_\alpha + \vec{S}_\beta$. The total angular momentum is then $\vec{J} = \vec{L} + \vec{S}$.

These vectors can be related to the $\vec{j}\cdot\vec{j}$ coupling vectors of equations 3.27 by the use of the 9j symbols.[91] The relationship is as follows:

$$|\ell_\alpha \tfrac{1}{2} \ell_\beta \tfrac{1}{2} LSJ> = \sum_{j_\alpha j_\beta} [(2S+1)(2L+1)(2j_\alpha+1)(2j_\beta+1)]^{\frac{1}{2}} \begin{Bmatrix} \frac{1}{2} & \frac{1}{2} & S \\ \ell_\alpha & \ell_\beta & L \\ j_\alpha & j_\beta & J \end{Bmatrix} | j_\alpha j_\beta J>. \tag{3.31}$$

The results for total angular momentum and parity $J^\pi = 1^-$ are

$$|0\tfrac{1}{2}\ 1\tfrac{1}{2}\ 101> = -\frac{\sqrt{3}}{3} |\ \tfrac{1}{2}\tfrac{1}{2}1>\ + \frac{\sqrt{6}}{3} |\ \tfrac{3}{2}\tfrac{1}{2}1>$$
$$|0\tfrac{1}{2}\ 1\tfrac{1}{2}\ 111> = \frac{\sqrt{6}}{3} |\ \tfrac{1}{2}\tfrac{1}{2}1>\ + \frac{\sqrt{3}}{3} |\ \tfrac{3}{2}\tfrac{1}{2}1> \tag{3.32}$$

The results for total angular momentum and parity $J^\pi = 2^+$ are

$$|0\tfrac{1}{2}\ 2\tfrac{1}{2}\ 202> = -\frac{\sqrt{10}}{5} |\ \tfrac{3}{2}\tfrac{1}{2}2>\ + \frac{\sqrt{15}}{5} |\ \tfrac{5}{2}\tfrac{1}{2}2>$$
$$|0\tfrac{1}{2}\ 2\tfrac{1}{2}\ 212> = \frac{\sqrt{15}}{5} |\ \tfrac{3}{2}\tfrac{1}{2}2>\ + \frac{\sqrt{10}}{5} |\ \tfrac{5}{2}\tfrac{1}{2}2> \quad . \tag{3.33}$$

The two cases leading to the relation $a_3 = -a_1$ are obtained by either $|0\tfrac{1}{2}1\tfrac{1}{2}111>$ or $|0\tfrac{1}{2}2\tfrac{1}{2}212>$ being equal to zero. Studies with polarized protons indicate that $|0\tfrac{1}{2}1\tfrac{1}{2}111>$ is non-zero.[92] As seen by previous experimenters [15,19,33]

the contribution of the spin flip terms $|0\frac{1}{2}1\frac{1}{2}11\rangle$ and $|0\frac{1}{2}2\frac{1}{2}12\rangle$ to the un-polarized cross section is zero to within the experimental error. The data in this experiment are consistent with neglecting spin-flip as can be seen in Figure 2.7 and 3.3. Therefore, these terms were not included in the analysis.

Results

The experimental data is consistent with the assumption that the reaction is dominated by the electric dipole radiation. Considering only electric dipole and quadrupole radiation, the magnitude of the cross section for $\theta_{cm} = 90^{o}$ is a measure of the electric dipole strength if the angular distribution of the quadrupole radiation is of the form of the spherical harmonic Y_{21} (which vanishes at 90^{o}). Using these assumptions, an empirical equation for the electric dipole strength was derived from the experimental data, using a linear least squares fit to the experimental $^{3}H(p,\gamma)^{4}He$ cross section between 23 and 42 MeV excitation. The cross section in this energy range was found to be best represented by a cubic polynomial with a reduced chi-square of 0.02. The resulting expression for the E1 radiation in the model is

$$D_1^2 = \frac{4m_p c^2 E_p}{E_\gamma^2}\{1.518\times10^{-3}+3.953\times10^{-4}E_x-3.921\times10^{-5}E_x^2+5.419\times10^{-7}E_x^3\} \qquad (3.34)$$

This expression gives the 90^{o} cross section shown as the solid curve in Figure 2.5. Using this result for D_1 , the model parameters were obtained to produce the solid curves in Figure 2.6 for the angles $\theta_{cm} = 53^{o}, 123^{o}$. The asymmetry ($a_s$) resulting from this calculation is displayed as the solid curve in Figure 3.2. The parameters of the calculation are shown in Table 3.1 for the resonances observed in the data.

Table 3.1

Direct and Resonance Parameters of the E2 Cross Section

E(Mev)*	Γ_γ(keV)	Γ_p(MeV)	η	δ_1	$\alpha_2(\frac{mb}{MeV^{1/2}})^{1/2}$	δ_2
35.	2.6	12.8	50^{o}	-65^{o}	1.24×10^{-4}	-46^{o}
39.5	0.60	3.2	35^{o}			

*all energies are cm

The least squares fits to the angular distributions are shown in Figure 2.7 as the solid lines. The coefficients for the Legendre polynomials as a function of the incident proton energy at the center of the target are displayed in Table 3.2. The Legendre coefficients obtained from the excitation curve analysis are shown as the solid curves on Figure 3.3 overlaid with the experimental results. The experimental results are shown to support the hypothesis that $a_3 = -a_1$ and $1+a_2+a_4=0$ to within experimental error at all measured energies with the exception of E_p = 23.0 MeV. The agreement between

Figure 3.2 Asymmetry of the $^{3}H(p,\gamma)^{4}He$ Angular Distribution. The asymmetry data from the measurements at $\theta_{cm} = 55^{o}$ and 125^{o} are the solid dots with the error bars showing the statistical error. The asymmetry from the angular Distribution of Figure 2.7 are shown as x's with arrowheads indicating the error propagated from a_1 and a_3. The results reported by previous experimenters is also plotted.[13,60,58]

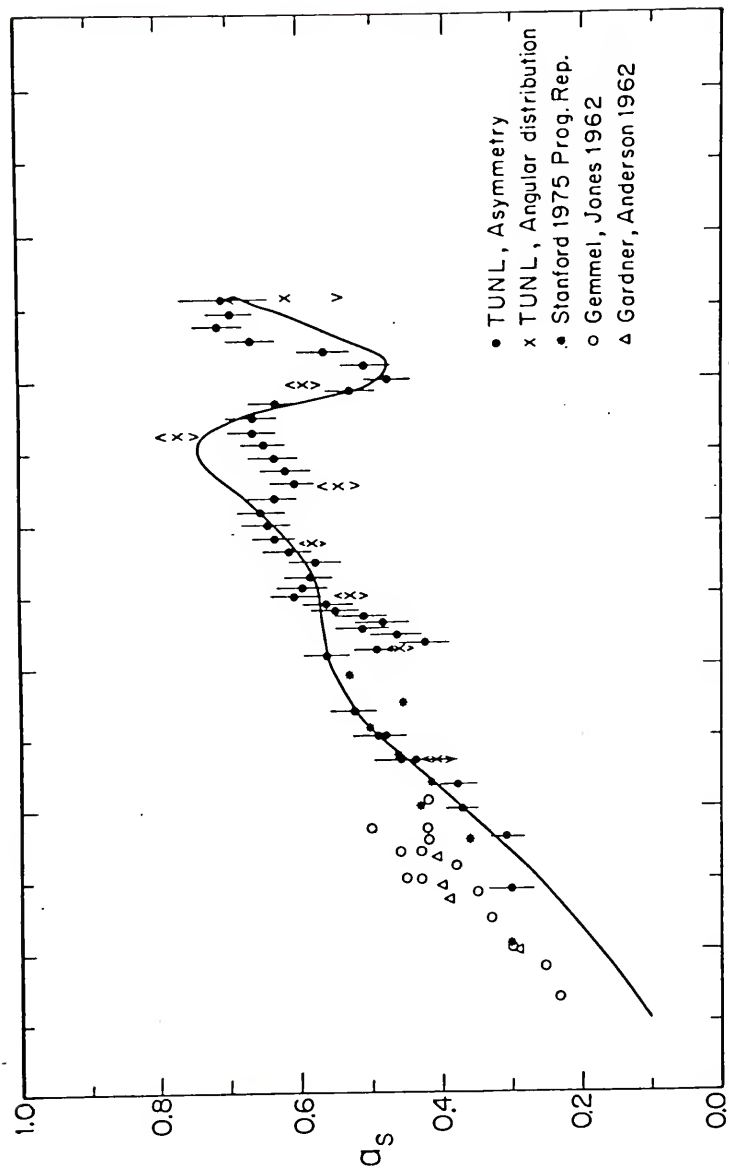
• TUNL, Asymmetry
x TUNL, Angular distribution
• Stanford 1975 Prog. Rep.
o Gemmel, Jones 1962
Δ Gardner, Anderson 1962
a_s
E_γ (MeV)
1.0
0.8
0.6
0.4
0.2
0.0
20
24
28
32
36
40
44
48

Table 3.2

a_i Coefficients of Measured Angular Distributions for $^3H(p,\gamma)^4He$

E_γ	A_o	a_1	a_2	a_3	a_4
MeV	$\mu b/_{Sr}$				
29.4	5.40 ± .17	0.243 ± 0.018	- 0.908 ± 0.021	- 0.247 ± 0.022	- 0.106 ± 0.066
32.4	4.54 ± .13	0.273 ± 0.009	- 0.936 ± 0.013	- 0.279 ± 0.009	- 0.075 ± 0.025
33.9	4.27 ± .10	0.314 ± 0.009	- 0.825 ± 0.012	- 0.309 ± 0.009	- 0.180 ± 0.013
35.4	3.79 ± .09	0.348 ± 0.010	- 0.893 ± 0.013	- 0.337 ± 0.009	- 0.104 ± 0.016
36.8	3.36 ± .06	0.292 ± 0.008	- 0.868 ± 0.011	- 0.370 ± 0.008	- 0.028 ± 0.024
38.3	2.96 ± .06	0.458 ± 0.009	- 0.798 ± 0.011	- 0.466 ± 0.009	- 0.189 ± 0.010
39.8	2.69 ± .06	0.353 ± 0.009	- 0.841 ± 0.012	- 0.359 ± 0.009	- 0.174 ± 0.012
42.0	3.16 ± .21	0.382 ± 0.070	- 0.890 ± 0.071	- 0.350 ± 0.073	- 0.084 ± 0.175

Figure 3.3 Coefficients of the Legendre Expansion of $\sigma(\theta)$. The a_i coefficients from the angular distributions of Figure 2.7 are shown as x's in the upper plot. The error bars are the errors of the coefficients a_i obtained from the least squares fit of the data to the Legendre expansion. The lower plot shows the experimental A_o obtained from the cross sections of Figure 2.6. The solid curves in both plots are the results obtained from the model (Equation 3.10). The energy E_γ is in the center of mass.

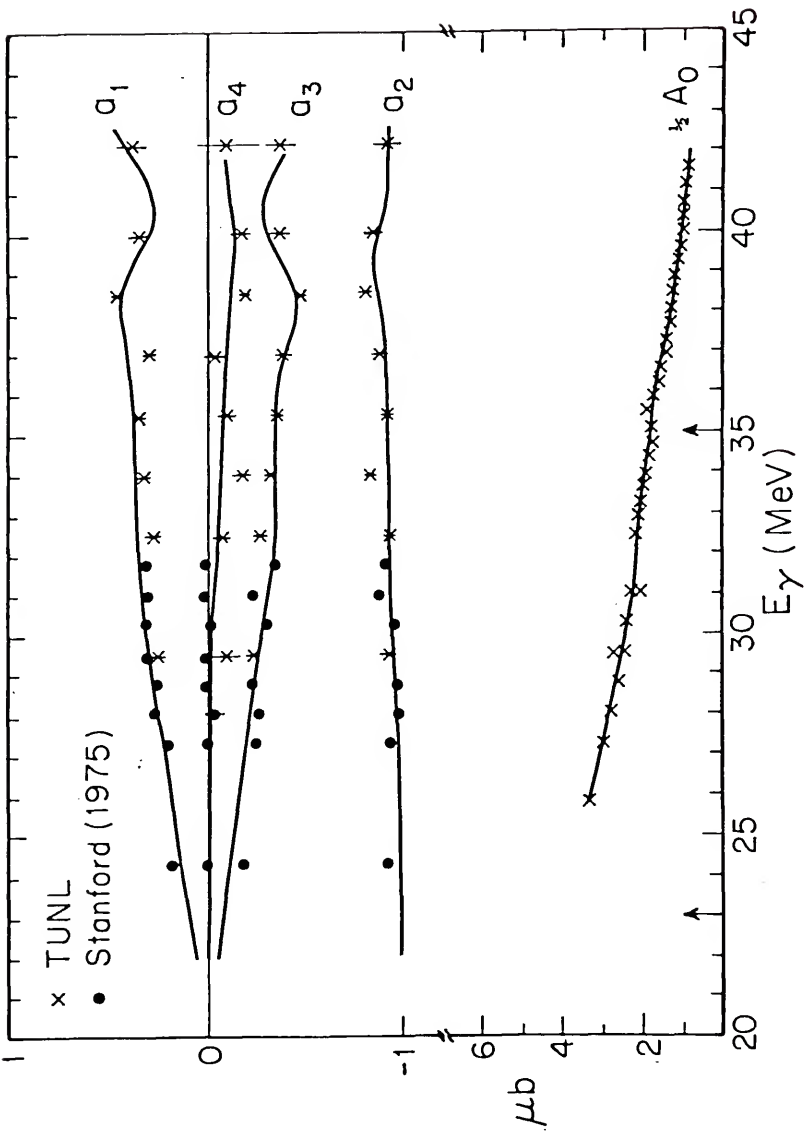
× TUNL
• Stanford (1975)
a_1
a_4
a_3
a_2
½ A_0
1
0
-1
6
4
2
μb
20
25
30
35
40
45
E_γ (MeV)

the experimental data and the model of direct E2 and two E2 resonances superimposed on a dominant E1 background interaction is seen to be quite satisfactory.

For comparison to theoretical calculations in the literature, the integrated cross sections due to the individual components of the model were evaluated. The total photonuclear cross section is obtained by integrating the Legendre polynomial expansion of the angular distribution (Equation 1.4) over all solid angles. The result is

$$\int d\Omega \ \frac{d\sigma}{d\Omega} = 4\pi A_o = B_o + B_2 = \sigma^{E1} + \sigma^{E2}$$

where B_o and B_2 are defined by Equation 3.21. As seen in Equation 3.21, the individual contributions of the direct and resonance terms used in the model may be evaluated separately. The results of this evaluation are shown in Table 3.3.

Table 3.3

Cross Sections Integrated From 22 to 44 MeV Excitation

$\int \sigma_{\gamma,p}\, dE = 30.6$ mb MeV	$\int \sigma^{E1}\, dE = 29.6$ mb MeV
$\int \sigma^{E2}\, dE = 1.01$ mb MeV	$\int \frac{\sigma^{E2}}{E^2}\, dE = 8.12 \times 10^{-4}$ mb/MeV
$\int R_1^2\, dE = 0.226$ mb MeV	$\int \frac{R_1^2}{E^2}\, dE = 1.78 \times 10^{-4}$ mb/MeV
$\int R_2^2\, dE = 0.047$ mb Mev	$\int \frac{R_2^2}{E^2}\, dE = 3.07 \times 10^{-4}$ mb/MeV
$\int \sigma_d^{E2}\, dE = 0.969$ mb MeV	$\int \frac{\sigma_d^{E2}}{E^2}\, dE = 6.69 \times 10^{-4}$ mb/MeV

SUMMARY AND CONCLUSION

The TUNL Cyclo-Graaff was used to obtain data from the $^{3}H(p,\gamma)^{4}He$ reaction for protons of energies from 8-30 MeV in the laboratory. The data were taken as a series of excitation curves and angular distributions. The data obtained can be adequately accounted for if the radiation is viewed as being predominantly electric dipole with an admixture of direct and resonant electric quadrupole radiation. Two electric quadrupole resonances are observed and the resonance width obtained for each. The resonance at a compound nucleus excitation of 35 MeV with a width of 12 MeV is in good agreement with the result reported by Malcom, et al.[22] in the ^{4}He photoneutron experiments at the Saskatchewan Linear Accelerator Laboratory. A second, previously unobserved, resonance is seen with a width of $\sim$3.2 MeV at an excitation energy of 39.5 MeV. A survey of the experimental literature shows a possible indication of structure at this energy in the $^{4}He(\gamma,d)^{2}H$ reaction measurements reported by Skopik and Dodge[69] and in $^{4}He(\gamma,p)^{3}H$ assymetry measurements by Arkatov, et al.,[19] thus lending credibility to the result reported here.

The observed resonances are in good agreement with the $(J^{\pi},T) = (2^{+},0)$ and $(2^{+},1)$ levels reported by Szydlik, et al.[36] for shell model calculations with modified Sussex[93] potentials, where T is the isospin quantum number.[94] This reference quotes levels of $(2^{+},0)$ located at about 34 MeV and $(2^{+},1)$ located at about 44 MeV excitation. The integrated strengths of these two levels are reported as 0.86 and 0.96 mb MeV respectively giving a total E2 strength of 1.86 mb MeV from threshold to 50 MeV. This strength compares with 0.23 and 0.047 mb MeV for the two levels observed and 0.97 mb MeV for the E2 direct term. The total E2 strength from this experiment is found to be 1.01 mb MeV (Table 3.3).

The above reference would imply that the newly observed level at 39.5 MeV would have an isospin assignment of T = 1. A definite assignment of the isospin quantum number can not be made from this experiment as both T = 0 and T = 1 quadrupole states can be formed in the $^{3}H(p,\gamma)^{4}He$ reaction. The narrow width, however, suggests the T = 1 assignment since fewer decay channels are available.

A recent microscopic continuum calculation by Bevelacqua and Philpott[95] indicates a $(2^{+},0)$ resonance of 3.8 MeV width at about 39 MeV in ^{4}He. Bevelacqua and Philpott compare this level to the experimental data of Lin, et al.[96] Using inelastic scattering of deuterons from

^{4}He and ^{6}Li, Lin and Associates suggest the existence of a level of width from 2.8 to 5.6 MeV at an excitation energy of 31.7 MeV to fit the trend of their data at the upper end of their observed energy range. Since the data of Lin, et al. includes only the low energy tail of this resonance, their width assignment of this level must remain questionable. While it is tempting to associate this narrow level with the level observed at 39.5 MeV in this experiment, the level at 35 MeV observed both here and by Malcom, et al.[22] cannot be ignored. If the level in the reported calculation of Bevelacqua and Philpott corresponds to the 35 MeV resonance observed here, then their level corresponding to the 39.5 MeV resonance would be at an energy beyond the range of their calculation.

It is apparent that further theoretical work is necessary in order to explain and understand the existence of the 2^{+} level at 39.5 MeV observed in this experiment. This series of experiments extends the energy range covered by the $^{3}H(p,\gamma)^{4}He$ reaction measurements from 18 to 30 MeV incident proton energy. The (p,γ) reaction lends itself to better resolution and simpler analysis than the $^{4}He(\gamma,p)^{3}H$ or $^{4}He(e,e'p)^{3}H$ experiments that comprise the data in the literature in this energy range. The effects of an E2 component in the radiation are seen in the measured angular distributions.

APPENDIX A

The spectra for each energy and angle measurement were written on magnetic tape for off line computer analysis. The spectra were fit to the response curve of the detector for monochromatic γ-ray. This response curve was obtained by accumulating a $^{3}H(p,\gamma)^{4}He$ spectrum with 2741 counts in the full width at half maximum of the peak. A least squares fit to the spectrum was obtained for the composite function

$$F(x) = (1-\theta(x-C_9+\varepsilon)\exp(C_1+C_2x+C_3x^2+C_4x^3) + \theta(x-C_9-\varepsilon)\exp(C_5+C_6x+C_7x^2+C_8x^3)$$

where

$$\theta(x-x_o) = \begin{cases} 0 & x < x_o \\ 1 & x \geq x_o \end{cases}$$

and $x_o = C_9$ is the channel where the two functions have equal magnitude and slope.[97] The first term is the low energy tail of the peak and the second is the peak and high energy edge of the spectrum. The coefficients C_i obtained from this fit determined the standard curve shape. The experimental measurements were then fit to the equation

$$F(X) = B\,(1-\theta(X-C_9+\varepsilon)\exp(C_1+C_2X+C_3X^2+C_4X^3) + \theta(X-C_9-\varepsilon)\exp(C_5+C_6X+C_7X^2+C_8X^3)$$

where $X = \frac{x-P}{R} + X_{max}$. The fitting parameters are the amplitude B, the gain R and the peak position P. The variable x corresponds to the channel numbers, and the term X_{max} is the peak of the standard spectrum. The fitting is done by a parabolic extrapolation of the chi-squared hypersurface routine that is a modification of the routine Chifit described by Bevington.[98] This routine was found to be reasonably fast while yielding reproducable fits to the experimental spectra. The coefficients of the fitting equation are as follows:

$C_1 = 3.6393$ $\qquad$ $C_5 = 1.4269 \times 10^{3}$

$C_2 = 8.9808 \times 10^{-2}$ $\qquad$ $C_6 = 1.4674 \times 10^{1}$

$C_3 = 4.8943 \times 10^{-4}$ $\qquad$ $C_7 = 5.0242 \times 10^{-2}$

$C_4 = 9.1427 \times 10^{-7}$ $\qquad$ $C_8 = 5.7104 \times 10^{-5}$

$X_{max} = 312.5$ $\qquad$ $C_9 = 294.$

$R = (x_2 - x_1)\ 2.5 \times 10^{-2}$ $\qquad$ $B = N/95.$

The peak channel counts N, and half width $x_2 - x_1$ are initially selected by the operator using a light pen on the displayed spectrum.

A sample fit is shown in Figure A.1 for the gamma ray emitted at the laboratory angle of 65^{o} for an incident proton energy of 30 MeV.

Figure A.1 $^{3}H(p,\gamma)^{4}He$ Spectrum for 30 MeV Incident Proton Energy. The full energy peak, first escape peak, and second escape peak are indicated. The solid curve indicates the fit obtained using the peak fitting program

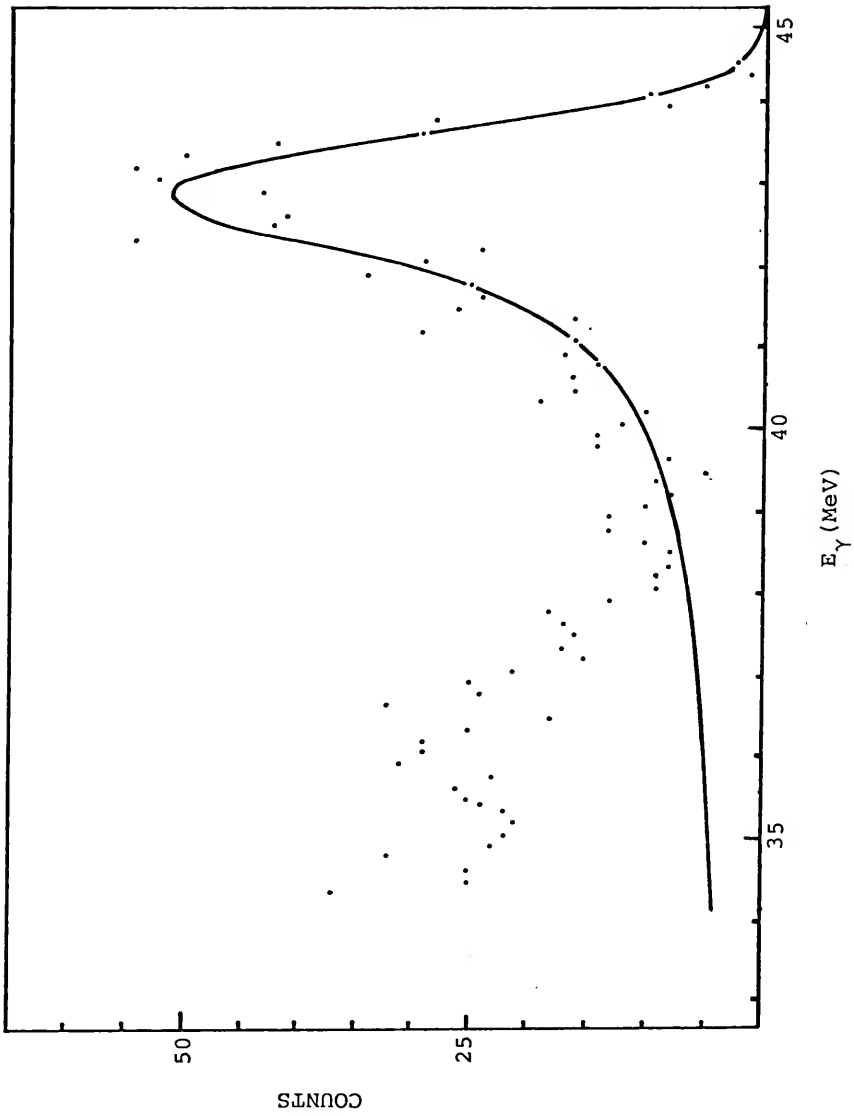
COUNTS
50
25
35
40
45
E_γ (MeV)

APPENDIX B

Table B.1

Experimental Angular Distributions*

E_γ	29.5	32.4	33.9	35.4
θ		26.	21.	21.
σ(θ)		2.34 ± .18	1.57 ± .15	1.41 ± .14
θ	44.	44.	44.	44.
σ(θ)	4.95 ± .20	4.48 ± .15	4.42 ± .15	4.14 ± .14
θ		52.	52.	52.
σ(θ)		5.63 ± .17	5.93 ± .17	4.80 ± .16
θ	57.			
σ(θ)	7.59 ± .25			
θ	72.	73.	73.	73.
σ(θ)	8.50 ± .27	7.17 ± .19	6.28 ± .18	5.47 ± .14
θ	82.			
σ(θ)	7.99 ± .27			
θ	92.	93.	93.	93.
σ(θ)	6.70 ± .24	6.02 ± .18	5.19 ± .17	4.78 ± .27
θ	112.	113.	113.	113.
σ(θ)	6.19 ± .24	4.86 ± .16	4.36 ± .16	3.85 ± .15
θ	127.	132.	132.	127.
σ(θ)	4.28 ± .20	2.80 ± .13	2.69 ± .12	2.50 ± .12
θ	143.	144.	144.	144.
σ(θ)	2.17 ± .14	1.74 ± .07	1.74 ± .10	1.33 ± .07

Table B.1 (continued)

E_γ	36.8	38.3	39.8	42.0
θ	21.	21.	21.	
σ(θ)	1.31 ± .13	1.42 ± .14	.86 ± .11	
θ	44.	44.	44.	
σ(θ)	3.43 ± .11	3.68 ± .11	3.18 ± .11	
θ	50.	50.	51.	51.
σ(θ)	3.86 ± .12	3.96 ± .12	3.45 ± .11	4.09 ± .18
θ	58.	58.	58.	61.
σ(θ)	4.80 ± .13	4.70 ± .13	3.92 ± .12	4.66 ± .14
θ	73.	73.	73.	68.
σ(θ)	6.68 ± .17	6.15 ± .17	5.00 ± .15	4.71 ± .14
θ				84.
σ(θ)				5.33 ± .22
θ	93.	93.	93.	97.
σ(θ)	4.34 ± .13	3.42 ± .11	3.29 ± .11	3.38 ± .19
θ	113.	113.	113.	113.
σ(θ)	3.24 ± .11	2.63 ± .10	2.86 ± .11	3.01 ± .12
θ	128.	128.	128.	128.
σ(θ)	2.28 ± .10	1.72 ± .08	1.68 ± .08	2.01 ± .10
θ	144.	144.	144.	144.
σ(θ)	1.32 ± .06	.99 ± .04	1.04 ± .05	.96 ± .07

* all entries are center of mass, cross sections are μb

BIBLIOGRAPHY

1. J. H. Mattauch, W. Thiele, and A. H. Wapstra, Nucl. Phys. 67 (1965) 1

2. R. W. McAllister and R. Hofstadter, Phys. Rev. 102 (1956) 851

3. H. Frank, D. Haas, and H. Prange, Phys. Lett. 19 (1965) 391

4. R. F. Frosh, J. S. McCarty, R. E. Rand and M. R. Yearian, Phys. Rev. 160 (1967) 874

5. G. R. Plattner, R . D. Viollier, and K. Alder, Phys. Rev. Lett. 34 (1975) 874

6. W. Czyz and L. Lesniak, Phys. Lett., 25B (1967) 319

7. D. Vinciguerra, Lett. Nuovo Cim. 10 (1974) 799

8. D. Mahanti, H. L. Yadov, and B. K. Srivastava, Nucl. Phys. A169 (1971) 76

9. J. S. Levinger, Nuclear Photodisintegration, Oxford U. Press, Oxford, England (1960) 97

10. A. N. Gorbunov, Phys. Lett. 27B (1968) 436

11. A. N. Gorbunov and V. M. Spiridonov, JETP (Sov. Phys.) 34 (1958) 596

12. G. D. Wait, S. K. Kundu, Y. M. Shin, and W. F. Stubbins, Phys. Lett. 33B (1970) 163

13. W. E. Meyerhof, M. Suffert, and W. Feldman, Nucl. Phys. A148 (1970) 211

14. L. Crone and C. Werntz, Nucl. Phys. A134 (1969) 161

15. S. Fiarman and W. E. Meyerhof, Nucl. Phys. A206 (1973) 1

16. R. Frosch, R. E. Rand, M. R. Yearian, H. L. Crannell, and L. R. Suelze, Phys. Lett. 19 (1965) 155

17. T. Walcher, Phys. Lett. 31B (1970) 442

18. C. Milone, Phys. Rev. 120 (1960) 1302

19. Y. M. Arkatov, P. I. Vatset, V. I. Voloshchuk, V. V. Kirichenko, I. M. Prokhorets, and A.F. Khodyachikh Sov. J. Nucl. Phys. 13 (1971) 142

20. J. E. Perry and S. J. Bame, Phys. Rev. 99 (1955) 1368

21. C. C. Gardner and J. D. Anderson, Phys. Rev. 125 (1962) 626

22. C. K. Malcom, D. V. Webb, Y. A. Shin, and D. M. Skopik, Phys. Lett. 47B (1973) 433

23. M. Gari and H. Hebach, Phys. Rev. C10 (1974) 1629

24. R. Leonoardi and M. Rosa Clot, Riv. Nuouvo Cim. 1 (1971) 1

25. L. H. Thomas, Natuurwiss 13 (1925) 625

26. W. Kuhn, Zeits. Phys. 33 (1923) 408

27. L. Ladenburg and F. Reiche, Natuurwiss 11 (1923) 873

28. J. S. Levinger and H. A. Bethe, Phys. Rev. 78 (1950) 115

29. R. Hermann and R. Hofstadter, High-Energy Electron Scattering, Stanford, Cal., (1960) 62

30. L. L. Foldy, Phys. Rev. 107 (1957) 1303

31. D. Frerejacque, D. Benaksas and D. Drickey, Phys. Rev. 141 (1968) 1308

32. Ya. M. Arkatov, A. V. Bazaeva, P. I. Vatset, V. I. Voloshchuk, A. P. Rlyncharev and A. F. Khodyachikh, Sov. J. Nucl. Phys. 10 (1970) 639

33. Yu. M. Arkatov, P. I. Vatset, V. I. Voloshchuk, V. V. Kirichenko, I. M. Prokhorets, and A. F. Kohdyachikh, Sov. J. Nucl. Phys. 12 (1971) 123

34. W. E. Meyerhof, W. Feldman, S. Gilbert and W. O'Connell, Nucl. Phys. A131 (1969) 489

35. P. Quarati, Nucl. Phys. A115 (1968) 651

36. P. P. Szydlik, J. R. Borysowicz and R. F. Wagner, Phys. Rev. C6 (1972) 1902

37. W. E. Meyerhof and S. Fiarman, Intn'l. Conf. on Photonuclear Reactions and Applications, Pacific Grove (1973) 385

38. R. Leonardi and E. Lipparini, Phys. Letts. 47B (1973) 385

39. H. Frosch, Phys. Lett. 37B (1971) 140

40. S. Radhakant, S. B. Khadkikar and B. Banerjee, Nucl. Phys. A142 (1970) 81

41. C. A. Malcom, Ph.D. Thesis University of Saskatchewan (1972)

42. C. Noguchi and F. Prats, Phys. Rev. Lett. 33 (1974) 1168

43. G. A. Ferguson, J. Halpern, R. Nathans and P. F. Yergin, Phys. Rev. 95 (1954) 776

44. G. de Saussure and L. S. Osborne, Phys. Rev. 99 (1955) 843

45. D. L. Livesey and I. G. Main, Nuovo Cim. 10 (1958) 590

46. L. Ferrero, Nuovo Cim.45B (1966) 273

47. Y. M. Arkatov, P. I. Vatset, V. I. Voloschuk, A. P. Klyucharev, V. L. Marchenko, and A. F. Khodyachikh, Sov. J. Nucl. Phys. 9 (1969) 271

48. L. Busso, S. Costa, L. Ferrero, R. Garfagini. L. Pasqualini, G. Piragino, S. Ronchi Della Rocca and A. Zanini, Nuovo Cim. Lett. 33B (1970) 163

49. L. Busso, Nuovo Cim. Lett. 3 (1970) 423

50. B. L. Berman, S. C. Fultz and M. A. Kelley, Phys. Rev. Lett. 25 (1970) 938

51. B. L. Berman, S. C. Fultz and M. A. Kelley, Phys. Rev. C4 (1971) 723

52. B. L. Berman, F. W. K. Firk and C. P. Wu, Nucl. Phys. A179 (1972) 791

53. J. D. Irish, R. G. Johnson, B. L. Berman, B. J. Thomas, K. G. McNeill and J. W. Jury, Phys. Rev. C8 (1973) 433

54. J. D. Irish, R. G. Johnson, B. L. Berman, B. J. Thomas, K. G. McNeill and J. W. Jury, Can. J. Phys. 53 (1975) 802

55. Y. M. Arkatov, P. I. Vatset, V. I. Voloschuk, V. N. Gurev, V. A. Zolenko, I. M. Prokhorets and V. I. Chmil, Sov. J. Nucl. Phys. 21 (1976) 475

56. J. E. Perry and S. J. Bame, Phys. Rev. 90 (1963) 380

57. R. Schrack, D. Kohler, N. G. Puttaswamy and W. E. Meyerhof, Phys. Lett. 18 (1965) 327

58. D. S. Gemmel and G. A. Jones, Nucl. Phys. 33 (1962) 102

59. J. P. Didelez, H. Langevin, Joliot, P. Narboni and G. Chretien, Few Body Problems, Light Nuclei and Nuclear Interactions, N.Y. Gordon and Breach, New York, USA (1968) 733

60. H. F. Glavish, C. C. Chang, S. S. Hanna, R. Avida and W. E. Meyerhof, Few Particle Problems in the Nuclear Interaction, North-Holland Publishing Co., Amsterdam, Holland (1972) 631

61. L. Busso, R. Garfagnini, G. Piragino, S. Ronchi Della Rocca and A. Zanini, Lett. al Nuovo Cim. 1 (1971) 941

62. P. E. Argan, G. Audit, N. de Bottom, J. L. Faure, J. M. Laget, J. Martin, C. G. Schul and G. Tamas, Nucl. Phys. A237 (1975) 447

63. W. R. Dodge and J. J. Murphy II, Phys. Rev. Lett. 28 (1972) 839

64. E. G. Fuller, Phys. Rev. 96 (1954) 1306

65. I. G. Main, Nuovo Cim. 26 (1962) 884

66. H. G. Clerc, R. J. Stewart and R. C. Morrison, Phys. Lett. 18 (1965) 316

67. R. Mundhenke, R. Kosick and G. Kraft, Z. Phys. 216 (1968) 232

68. V. F. Denisov and L. A. Kulchitskii, Sov. J. Nucl. Phys. 6 (1968) 318

69. D. M. Skopik and W. R. Dodge, Phys. Rev. C6 (1972) 43

70. J. G. Ashbury and F. J. Loeffler, Phys. Rev. B137 (1965) 1214

71. Y. M. Arkatov, P. I. Vatset, V. I. Voloshchuk, I. M. Prokhorets, A. F. Khodyachikh and V. I. Chmil, Sov. J. Nucl. Phys. 16 (1973) 6

72. Y. K. Akimov, O. V. Shevchenko and L. M. Soroko, Sov. Phys. JETP 14 (1962) 512

73. J. A. Poirer and M. Pripstein, Phys. Rev. 130 (1963) 1171

74. R. W. Zurmuhle, W. E. Stephens and H. H. Staub, Phys. Rev. 132 (1963) 751

75. A. Degre, M. Schaeffer and M. Suffert, J. Physique C5 (1971) 221

76. J. M. Poutissou and W. Del Bianco, Nucl. Phys. A199 (1973) 517

77. J. T. Londergan and C. M. Shakin, Phys. Rev. Lett. 28 (1972) 1729

78. A. H. Chung, R. G. Johnson and J. W. Donnelly, Nucl. Phys. A235 (1974) 1

79. B. F. Gibson, Nucl. Phys. A195 (1972) 449

80. J. D. Irisn, R. G. Johnson, K. G. McNeill and J. W. Jury, Phys. Rev. C9 (1974) 2060

81. J. M. Blatt and L. C. Biedenharn, Rev. Mod. Phys. 24 (1952) 258

82. H. R. Weller, R. A. Blue, N. R. Roberson, D. G. Rickel, S. Maripuu, C. P. Cameron, R. D. Ledford, and D. R. Tilley, Phys. Rev. C13 (1976) 922

83. Nukem, GmbH, D-6450, Hanau 11

84. J. J. Jackson, Classical Electrodynamics, John Wiley & Sons, Inc., New York (1962) 401

85. J. B. Marion, Classical Dynamics of Particles and Systems, Academic Press, Inc., New York (1970) 306

86. Evans Hayward, Nuclear Structure and Electromagnetic Interactions, N. McDonald, Ed., Plenum, New York (1965) 141

87. B. Buck, R. N. Maddison and P. E. Hodgson, Phil. Mag. 5 (1960) 1181

88. B. H. Flowers and F. Mandl, Proc. Roy. Soc. A206 (1951) 31

89. A. J. Ferguson, Angular Correlation Methods in Gamma Ray Spectroscopy, North-Holland, Amsterdam (1965)

90. J. Als-Nielsen, Newsletter No. 6, Neutron Data Compilation Center European Nuclear Energy Agency, Gif-sur-Yvette, France (September 1967) 9

91. I. E. McCarthy, Introduction to Nuclear Theory, John Wiley & Sons, Inc., New York (1968) 528

92. G. King, E. Wienhard, M. Sasao, J. Calarco, S. S. Hanna and H. F. Glavish, Stanford University Progress Report (1977) 9 (Unpublished)

93. J. P. Elliott, A. D. Jackson, H. A. Mavromatis, E. A. Sanderson, and B. Singh, Nucl. Phys. A121 (1968) 241

94. L. Eisenbud and E. P. Wigner, Nuclear Structure, Princeton University Press, Princeton (1958) 39

95. J. J. Bevelacqua and R. J. Philpott, Nucl. Phys. A275 (1977) 301

96. E. K. Lin, R. Hazelberg and E. L. Haase, Nucl. Phys. A179 (1972) 65

97. L. Blatt, Private Communication

98. P. R. Bevington, Data Reduction and Error Analysis for the Physical Sciences, McGraw-Hill, Inc., New York (1969) 226

BIOGRAPHY

The place of my birth is Magdalena, New Mexico, and the date was May 24, 1947. I am the eldest of four children. I attended the Quemado, New Mexico, grade school until the seventh grade when my family moved to Robert Lee, Texas, where I completed my primary and secondary education in the Robert Lee Schools. I played the flute in the high school band and was elected to the Beta Club National Honor Society. In May, 1964, I graduated second in a class of twenty-two. After graduating from high school, I entered San Angelo College, later to become Angelo State University. I was a member of the college band, was elected into Alpha Chi National Honor Society, and was awarded a Certificate of Scholastic Excellence. In June, 1968 I was awarded the degree of Bachelor of Science with a major in physics. Upon being awarded a NASA Traineeship by Illinois Institute of Technology, I entered Graduate School. While attending IIT, I met my wife to be. When I had completed the requirements for the degree of Master of Science at IIT, I transferred with my new bride to the University of Florida to complete my education.

I certify that I have read this study and that in my opinion it conforms to acceptable standards of scholarly presentation and is fully adequate, in scope and quality, as a dissertation for the degree of Doctor of Philosophy.

H. R. Weller, Chairman
Associate Professor of Physics

I certify that I have read this study and that in my opinion it conforms to acceptable standards of scholarly presentation and is fully adequate, in scope and quality, as a dissertation for the degree of Doctor of Philosophy.

R. A. Blue
Associate Professor of Physics

I certify that I have read this study and that in my opinion it conforms to acceptable standards of scholarly presentation and is fully adequate, in scope and quality, as a dissertation for the degree of Doctor of Philosophy.

T. L. Bailey
Professor of Physics

I certify that I have read this study and that in my opinion it conforms to acceptable standards of scholarly presentation and is fully adequate, in scope and quality, as a dissertation for the degree of Doctor of Philosophy.

J. W. Dufty
Associate Professor of Physics

I certify that I have read this study and that in my opinion it conforms to acceptable standards of scholarly presentation and is fully adequate, in scope and quality, as a disseration for the degree of Doctor of Philosophy.

G. R. Dalton

G. R. Dalton
Professor of Nuclear Engineering Sciences

This disseration was submitted to the Graduate Faculty of the Department of Physics in the College of Arts and Sciences and to the Graduate Council, and was accepted as partial fulfillment of the requirements for the degree of Doctor of Philosophy.

August 1977

Dean, Graduate School